https://doi.org/10.5194/egusphere-2025-6213
Preprint. Discussion started: 5 February 2026

Fire carbon emission constraints from space-based carbon monoxide retrievals during the 2019 intense burning season in Brazil

Anne-Wil van den Berg[1], Joram J. D. Hooghiem[1], Auke M. van der Woude[1], Pieter Rijsdijk[2,3,4], Roland Vernooij[1], Santiago Botía[5], Guido R. van der Werf[1], John B. Miller[6], Ingrid T. Luijkx[1], Maarten C. Krol[1,7], and Wouter Peters[1,8]

[1]Meteorology and Air Quality group, Wageningen University and Research, Wageningen, the Netherlands
[2]Space Research Organization Netherlands, Leiden, the Netherlands
[3]Satellite Observations department, Royal Netherlands Meteorological Institute, De Bilt, the Netherlands
[4]Department of Earth Sciences, Vrije Universiteit, Amsterdam, the Netherlands
[5]Department of Biogeochemical Signals, Max Planck Institute for Biogeochemistry, Jena, Germany
[6]Carbon Cycle Greenhouse Gases Division, National Oceanic and Atmospheric Administration Global Monitoring Laboratory, Boulder Colorado, United States of America
[7]Institute for Marine and Atmospheric Research, Utrecht University, Utrecht, the Netherlands
[8]Centre for Isotope Research, University of Groningen, Groningen, the Netherlands

Correspondence: Anne-Wil van den Berg (anne-wil.vandenberg@wur.nl)

https://doi.org/10.5194/egusphere-2025-6213
Preprint. Discussion started: 5 February 2026

Abstract.

In 2019, Brazil experienced an intensive fire season, despite the absence of major climate anomalies to enhance fire activity. Existing carbon monoxide (CO) emission estimates from state-of-the-art fire emission inventories differ by a factor two for the period and region. We provide a top-down estimate on CO emissions from these fires using the new CarbonTracker Europe – Long/Short Window (CTE-LW/SW) inverse modelling framework driven by column-averaged dry air CO mole fractions (X_{CO}) from the MOPITT and TROPOMI satellite instruments.

Our analysis indicates that the 2019 fires in Brazil released approximately 47 TgCO. Although structural atmospheric-chemistry related uncertainties remain (±15 TgCO), the inversions converged strongly to a common posterior (46–48 TgCO) independent of the prior emission inventory (GFED5.1, GFAS v1.2) or assimilated dataset (TROPOMI, MOPITT).

Posterior fire emissions closely resemble the newly released GFED5.1, supporting recent advances in bottom-up fire modelling. Nonetheless, at the biome level, our results reveal a systematic underestimation—by roughly a factor of two—in the Cerrado and Caatinga savannas relative to both fire emission priors. While more targeted uncertainty assessments are required, we speculate that this emission gap unlikely stems from inversion choices alone and may indicate an underestimation of fuel loads or emission factors.

Overall, we demonstrate CTE-LW/SW effectively leverages X_{CO} to complement existing fire emission monitoring capacities at increasingly fine spatial resolution—a capability that is especially valuable in Brazil, where different fire regimes occur in close proximity and fire activity has intensified in recent years.

https://doi.org/10.5194/egusphere-2025-6213
Preprint. Discussion started: 5 February 2026

1 Introduction

In recent years, the Amazon region was subject to intense recurrent fires. These fires have far-reaching consequences for air quality, human health, biodiversity, and the regional carbon balance (e.g. Barlow et al., 2016; Nawaz and Henze, 2020; Friedlingstein et al., 2025). Fire disturbances further pressure the Amazon region to act as net sink, a capacity that growing evidence indicates is weakening (Gatti et al., 2021, 2023; Gloor et al., 2012; Brienen et al., 2015; Phillips et al., 2017; Hubau et al., 2020).

Unlike the adjacent fire-adapted and fire-dependent Cerrado savannas, Amazonian rainforests are not naturally shaped by fire (e.g. Cochrane, 2003; Pivello, 2011). Ignitions predominantly stem from human-driven land-use activities—primarily land clearing through slash-and-burn practices during which forest biomass is felled, dried, and then ignited (e.g. Uhl and Buschbacher, 1985; Morton et al., 2006, 2008). These intentional burns usually produce long-lasting, smouldering fires. Frequently, these escape into adjacent forests and persist as understory fires (e.g. Alencar et al., 2004, 2006; Morton et al., 2013), which contribute to forest degradation (Lapola et al., 2023). Both the deforestation fires themselves and the degradation that follows release large amounts of carbon into the atmosphere, impacting carbon cycling on immediate to multi-decadal timescales (e.g. van der Werf et al., 2017; Lapola et al., 2023; Qin et al., 2021; Bourgoin et al., 2024).

On top of anthropogenic pressures, environmental conditions, such as droughts, increase the susceptibility of the fire-sensitive Amazonian forests to burning (e.g. Brando et al., 2014). Dry seasons in Amazonia are becoming longer and more intense (Marengo et al., 2018; Wainwright et al., 2022). The forests increasingly experience drought–heatwave events that are more frequent, longer lasting, more extensive, and compounded by low soil moisture/high vapour-pressure deficit conditions (Ferreira et al., 2025). Climate projections from CMIP6 models indicate continued declines in rainfall, particularly in the southeastern Amazon, alongside hotter and longer droughts (Parsons, 2020; Ukkola et al., 2020). Fire-conducive weather conditions are becoming more frequent and extreme (Jolly et al., 2015; Jones et al., 2022), and projections indicate further increases—especially for extreme events (Jones et al., 2022). Even if the rate of deforestation declines, reductions in fire frequency (Le Page et al., 2017) and related carbon emissions (Aragão et al., 2018) are unlikely.

After more than a decade of declining deforestation rates, and in the absence of abnormal drought conditions, Amazonian fire activity rose sharply again in 2019. The fires drew the attention of the global media and scientists due to their scale and visibility (e.g. Silveira et al., 2020; Lizundia-Loiola et al., 2020; Brando et al., 2020a; Cardil et al., 2020; Kelley et al., 2021; Andela et al., 2022; Barlow et al., 2020; Escobar, 2019; Arruda et al., 2019), and rekindled concerns about increasing risks of large-scale forest dieback (Lovejoy and Nobre, 2019; Brando et al., 2020b). Fire emission estimates for this period were made, among others, by bottom-up fire emission models like the Global Fire Emissions Database (GFED van der Werf et al., 2017, 2025) and Global Fire Assimilation System (GFAS Kaiser et al., 2012), relying on burned area data coupled with a vegetation model or fire radiative power (FRP) data, respectively.

These fire emission models have advanced our understanding of fire dynamics and the emissions they produce. While significant progress has been made, important questions remain regarding their accuracy to estimate emission magnitudes, especially under challenging observational conditions (e.g. persistent cloud cover, below-canopy fires). A proper uncertainty

https://doi.org/10.5194/egusphere-2025-6213
Preprint. Discussion started: 5 February 2026

quantification therefore remains challenging. Through its co-release with carbon dioxide (CO_2) during incomplete combustion, carbon monoxide (CO) serves as tracer of fire activity. Fire-induced CO enhancements stand out against a relatively low background, making atmospheric CO observations a valuable proxy for total carbon emissions. Atmospheric modelling of CO provides an independent means to evaluate bottom-up fire inventories. When taken a step further through satellite driven inverse modelling, it can offer a powerful, complementary constraint on fire emissions.

Early atmospheric CO inversion studies relied on sparse surface measurements, which rarely captured fire plumes and thus placed little emphasis on optimizing fire emissions (Bergamaschi et al., 2000; Kasibhatla et al., 2002; Pétron et al., 2002; Pison et al., 2009; Hooghiemstra et al., 2011; Palmer et al., 2003), with the exception of a surface-based CO inversion by van der Werf et al. (2004), which despite its simplicity, proved effective in informing on continental scale fire emission anomalies and aided to improve the first global fire emissions data base (GFED) inventory estimates. The arrival of space-based CO retrievals—most notably from the Measurements of Pollution In The Troposphere (MOPITT), Tropospheric Emission Spectrometer (TES), and Infrared Atmospheric Sounding Interferometer (IASI) instruments—facilitated more systematic observations of fire plumes and brought fire emissions more to the forefront of inversion analyses. They especially helped to better understand the timing and magnitude of fire emissions (Heald et al., 2004; Pétron et al., 2004; Pfister et al., 2005; Arellano et al., 2006; Chevallier et al., 2009; Jones et al., 2009; Gonzi et al., 2011; Krol et al., 2013; Bloom et al., 2015; Yin et al., 2016; Nechita-Banda et al., 2018; Jiang et al., 2017; Zheng et al., 2018; Naus et al., 2022; Peiro et al., 2022; Zheng et al., 2023).

Advances in satellite retrieval algorithms and the introduction of new instruments such as the TROPOspheric Monitoring Instrument aboard ESA's Copernicus Sentinel-5 Precursor satellite (S5P-TROPOMI), constantly improve our capability to infer atmospheric CO abundances from space. These developments provide new opportunities to investigate fire emissions and their dynamics at increasingly higher spatial and temporal resolutions, as already demonstrated by for example van der Velde et al. (2021b, a); Byrne et al. (2021, 2024); Goudar et al. (2023); Nüß et al. (2025); Griffin et al. (2024); Forkel et al. (2025); Voshtani et al. (2025); Nguyen et al. (2023).

Despite these advances, few atmospheric CO inversion studies have focused specifically on South American fires (van der Laan-Luijkx et al., 2015; Bowman et al., 2017; Hooghiemstra et al., 2012; Naus et al., 2022), and none have studied the added value of TROPOMI observations for this region using a formal inversion. In this study, we provide fire CO emission estimates for the 2019 fires in Brazil using constraints from satellite column average CO mole fraction (X_{CO}) data using a novel inversion system. Our objectives are to (i) quantify the spatial and temporal distribution of CO fire emissions across different biome types, (ii) assess the consistency of TROPOMI constraints w.r.t. MOPITT, and (iii) evaluate fire emission modelling efforts for Brazilian fires with the inversion results. This work contributes to improve our understanding of the carbon impact of (extreme) fire events in the Amazon region to support future mitigation and monitoring strategies.

In the following sections, we first describe the new data assimilation framework and datasets used (Sect. 2). Subsequently, we demonstrate the performance of our system for the 2019 fire season, as an example of an intense fire year, by comparing our results with independent datasets (Sect. 3.1). We present the spatial and temporal overview of 2019 fire emissions (Sect. 3.2-3.3). We conclude with a discussion of our results and their implications for future fire emission quantification.

https://doi.org/10.5194/egusphere-2025-6213
Preprint. Discussion started: 5 February 2026

2 Methods and data description

2.1 The CTE-LW/SW inversion system for CO

To optimise South American fire emissions using satellite retrievals, we apply a two-step inversion framework consisting of a long-window (LW) and a short-window (SW) inversion. The LW inversion resolves monthly to inter-annual variability in the global CO budget, while the SW inversion targets daily variability in fire emissions. Decoupling the system in this way allows each step to use a set of observations that target spatio-temporal scales for source/sink processes of interest through the design of a statevector. We implement this approach in the CarbonTracker Data Assimilation Shell (CTDAS; van der Laan-Luijkx et al., 2017), building on the CarbonTracker Europe (CTE) ensemble Kalman smoother around the TM5 transport model (Peters et al., 2005).

The long-window inversion approach was recently developed for CO_2 and related tracers (van der Woude, 2024). Here, we present the first application that expands this LW system to CO. Subsequently, we designed and performed a short-window inversion for CO and refer to the combined system as CTE-LW/SW. We model atmospheric CO using the following the mass balance equation:

$$\frac{d\mathrm{CO}_{(x,y,z,t)}}{dt} = \overbrace{\lambda_{r,t}^{\text{fire}}}^{\text{short-window}} \cdot E_{(x,y,t)}^{\text{fire}} + \overbrace{\overbrace{\lambda_{r,t}^{\text{NMVOC}}} \cdot P_{(x,y,z,t)}^{\text{NMVOC}} + \overbrace{\lambda_{r,t}^{\text{CH}_4}} \cdot P_{(x,y,z,t)}^{\text{CH}_4} + \overbrace{\lambda_{r,t}^{\text{ant}}}}^{\text{long-window}} \cdot E_{(x,y,t)}^{\text{ant}} - L_{(x,y,z,t)}^{\text{CO+OH}} - D_{(x,y,t)}^{\text{dry}} \tag{1}$$

where E^{fire}, E^{ant} represent emissions from fires and anthropogenic activities. P^{NMVOC}, and P^{CH_4} stand for the chemical CO production through the oxidation of methane (CH_4) and non-methane volatile organic compounds (NMVOCs). Chemical loss of CO by the hydroxyl radical (OH; $L^{\text{CO+OH}}$) and dry deposition (D^{dry}) are calculated online in the atmospheric transport model that acts as observation operator (details in Sect. 2.3). The λ's represent a set of linear scaling factors for each source term for a given set of statevector elements (r) that are optimised in the indicated assimilation step (Table 1).

First, we optimise $\lambda_{r,t}^{\text{NMVOC}}$, $\lambda_{r,t}^{\text{CH}_4}$, and $\lambda_{r,t}^{\text{ant}}$ in the global-scale long-window inversion using flask observations from the National Oceanic and Atmospheric Administration Global Monitoring Laboratory (NOAA-GML) GLOBALVIEWplus v4.0 ObsPack (Schuldt et al., 2024). This step focuses on the capturing the monthly to inter-annual variation in the CO budget components (excluding fire emissions) using the background flask network. The long-window inversion then provides a set of optimised fluxes that serve as the prior for the second step: the short-window inversion. The short-window inversion optimises 3-daily scaling factors for fast varying fire emissions with satellite X_{CO} data that contain clear fire plume-like structures, while the other budget terms from the long-window optimisation are imposed.

A more detailed overview of the long-window inversion can be found in Appendix A1. The next sections further describe the short-window inversion configuration.

https://doi.org/10.5194/egusphere-2025-6213
Preprint. Discussion started: 5 February 2026

Table 1. Overview with the configuration of the CarbonTracker Europe Long-Window/Short-Window (CTE-LW/SW) inversions.

Component	**Long-window**	**Short-window**
Purpose	Optimise CO background	Optimise fire emissions
Assimilated observations	Flask samples from NOAA co_GLOBALVIEWplus_v4.0_2024-02-1 (Schuldt et al., 2024)	TROPOMI (Veefkind et al., 2012) or MOPITT (Drummond and Mand, 1996)
Statevector	λ^{CH_4}, λ^{NMVOC}, λ^{ant}	λ^{fire}
Time step / cycle length	1 month	3 days
n ensemble members	150	150
n lags	None	2
r statevector elements	6840 total, 95 per time step	2046
d.o.f.	115	77-108[1]
Inversion period	2014-2020	22 July - 30 Nov (2019)
Transport resolution	$6°\times4°\times25$ levels	$1°\times1°\times34$ levels

[1] d.o.f. varies per short-window inversion cycle due to our emission-dependent covariance pre-masking (Sect. 2.4)

2.2 Prior fire emissions from GFED5.1 and GFAS v1.2

We start our inversions from two distinct fire emission inventories: GFED5.1 (van der Werf et al., 2017, 2025) and the GFAS v1.2 (Kaiser et al., 2012). Burned area-based inventories, such as GFED (van der Werf et al., 2017), calculate emissions by combining satellite-based burned area with biogeochemical model outputs and emission factors. The new GFED5.1 inventory has improved detection of small fires by including higher-resolution burned area inputs from Chen et al. (2023) based on corrections derived mostly from Sentinel-2 and Landsat. Globally, this nearly doubled burned area estimates relative to MODIS alone. For Brazil this resulted in a 61% increase for 2019, particularly during the late dry season (July-Oct).

GFAS uses satellite-derived FRP observed by MODIS (both Terra and Aqua), to calculate fire emissions. Biome-level scaling factors based on GFED3 are used to convert fire radiative energy (FRE) to total dry matter burned (Heil et al., 2010), which are then combined with emissions factors that vary between biomes, mostly from Andreae and Merlet (2001), to calculate fire emissions.

All inventories use emission factors to convert total dry matter burned to trace gas emissions. Traditionally, these factors have been static biome averages while in reality they depend on fuel type, fuel moisture content, and meteorological conditions (van Leeuwen et al., 2013). Recently, Vernooij et al. (2023) combined a large set of savanna fire emission factor measurements across the world with geospatial proxies for these conditions (e.g. tree cover fraction, soil moisture, vapour pressure deficit) and a machine learning algorithm to derive dynamic savanna fire emission factors. GFED5.1 is the first inventory to operationally

https://doi.org/10.5194/egusphere-2025-6213
Preprint. Discussion started: 5 February 2026

introduce spatio-temporal dynamic emission factors for savanna fires that allow a more realistic representation of temporal and regional variability.

GFED5.1 and GFAS v1.2 yield considerably different emission estimates for the 2019 fire season in Brazil of 41 TgCO and 25 TgCO, respectively. Expressed as total carbon, this difference translates to a factor of roughly 1.5. At the biome scale, the contrasts become even more pronounced. In the Amazon biome, for example, the two inventories differ by up to a factor of two in both their CO and total carbon emissions. Beyond underscoring the need for observations, these differences provide a means to assess the robustness of our inversions by examining how the optimised emissions respond to each prior.

2.3 Atmospheric transport and chemistry

We use the Transport Model 5 Massive-Parallel (TM5-MP; Krol et al., 2005; Williams et al., 2017) model to transport the CO emissions and production fields, from which vertical profiles of CO mole fractions and pressure are sampled. These profiles, combined with averaging kernels, are subsequently used in CTDAS to derive X_{CO}.

The short-window TM5 simulations were performed globally at a horizontal resolution of $1°\times1°$, with 34 vertical levels, driven by three-hourly meteorological fields from the European Centre for Medium-Range Weather Forecasts (ECMWF) Reanalysis v5 (ERA5; Hersbach et al., 2020). Dry deposition is computed online. CO chemistry is linearised by prescribing three-hourly OH fields from the Copernicus Atmosphere Monitoring Service (CAMS) ECMWF Atmospheric Composition Reanalysis 4 (EAC4) dataset (Copernicus Atmosphere Monitoring Service, 2020; Inness et al., 2019), as well as the CO production from CH_4 and NMVOC oxidation optimised by the long-window. Fire emissions are distributed vertically using injection heights from the IS4FIRES dataset (Sofiev et al., 2012, 2013).

2.4 Statevector, covariance structure, and state propagation of the short-window system

Each statevector element (r) in $\lambda^{\mathrm{fire}}_{r,t}$ from equation (1) represents a 1°x1° grid box over land in South America between 22.5°S, 9.5°N, 79.5°W, and 34.5°W, resulting in a total of 1023 spatial unknowns (Fig. 1). At the start of each 3-day cycle, $\lambda^{\mathrm{fire}}_{r}$ are set to 1.0. We run the SW system with a 3-days assimilation window and 2 lags (i.e. 3-days lag). The scaling factors are optimised with a square root ensemble Kalman Smoother (Whitaker and Hamill, 2002; Peters et al., 2005). In each cycle, a total of (2×1023) optimised scaling factors are thus calculated in the SW inversion. The optimised mean state of each cycle is propagated to inform the next cycle's mean state. This mean state is determined as the average between the current cycle's optimised state and a state filled with λ values of 1.0 (which represent the prior fluxes that are calculated by the long-window system). This procedure ensures that the scaling factors quickly revert back to the unscaled prior value of 1.0 when no CO observations are present.

https://doi.org/10.5194/egusphere-2025-6213
Preprint. Discussion started: 5 February 2026

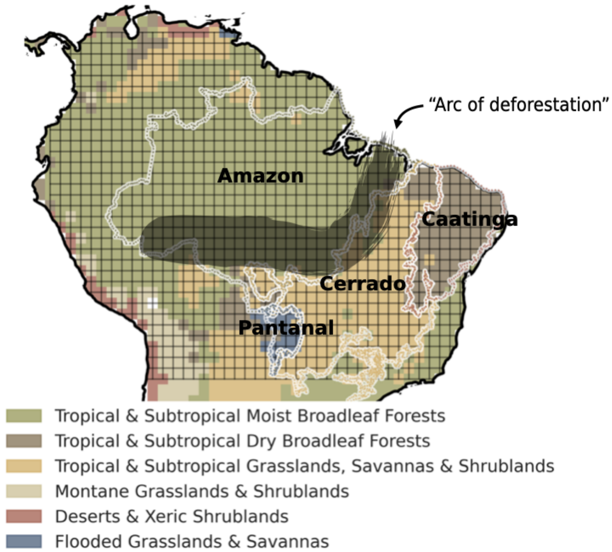

Figure 1. Region of interest for the short-window inversion. The grid lines represent the spatial definition of the short-window statevector. The background colours represent the biogeographical biome types, from Dinerstein et al. (2017), that we use in structuring the prior covariance matrix. The figure also outlines the biome definitions from the TerraBrasilis platform (TerraBrasilis, 2025) that we later use to analyse the fire emissions. The thick, semi-transparent, black line indicates the position of the arc of deforestation.

The degree of uncertainty on each scaling factor and their spatial correlations are described by the prior covariance structure. This covariance structure reflects our assumption that the errors in emission inventories are related to emissions factors and fuel characteristics or conditions, which often have some biome-dependency. We impose correlations within biogeographical biomes on using an e-folding distance correlation of 300 km (see also Fig. 1).

Given that only a subset of the gridded fire emission state contains non-zero values within a 3-day cycle, we restrict the state-space to these active grid cells. This targeted state reduction mitigates the impact of zero-signal elements, which can otherwise dilute the ensemble covariance estimate.

Fire emissions are inherently non-negative and represent a bounded quantity. However, in practice, the optimisation algorithm may generate negative λ values that correspond to physically impossible negative emissions. We apply a semi-exponential transformation (eq. 2), similar to Bergamaschi et al. (2009), to the optimized scaling factors where $\lambda < 1.0$. We acknowledge that this transformation introduces non-linearity in the relationship between the statevector deviations and X_{CO} deviations ($\mathbf{x}'$ and $\mathcal{H}(\mathbf{x}')$ respectively, see Peters et al. (2005)), yet we consider the use of the transformation to be more physically consistent, as it ensures the exclusion of unrealistic negative emissions. Besides, because we run a lagged system, subsequent lags can compensate for any non-linear effects introduced by this transformation.

$$\lambda = e^{(\lambda-1)} \qquad for\, \lambda < 1 \tag{2}$$

https://doi.org/10.5194/egusphere-2025-6213
Preprint. Discussion started: 5 February 2026

2.5 Observations for assimilation or validation

2.5.1 S5P-TROPOMI

The TROPOspheric Monitoring Instrument (TROPOMI) is a push-broom imaging spectrometer that measures backscattered solar radiances in the near-infrared (675–775 nm; NIR) and shortwave–infrared (2305–2385 nm; SWIR) (Veefkind et al., 2012). CO columns are retrieved using the shortwave infrared CO retrieval algorithm (SICOR Landgraf et al., 2016). The instrument is mounted on the Sentinel 5 Precursor (S5P) satellite. S5P was launched on October 13^{th} 2017 and flies in a sun-synchronous polar orbit at 824 km, crossing the equator at 13:30h LST. Due to its wide swath (2600 km across track), TROPOMI X_{CO} data covers Amazonia daily. At nadir, the columns have a footprint of 7×7 km^2 (before) or 5.5×7 km^2 (after) Aug. 6th 2019.

TROPOMI X_{CO} has extensively been validated against TCCON ground-based measurements and shown to meet the mission requirements of 10% precision and 15% accuracy (Borsdorff et al., 2018; Sha et al., 2021). Borsdorff et al. (2018) reported that, for clear-sky retrievals over land, biases are 6 ± 4 ppb, while Sha et al. (2021) found that, with recommended quality filtering, X_{CO} biases average $9\pm3\%$ across most TCCON stations. In addition, Martínez-Alonso et al. (2022) compared TROPOMI with the MOPITT archive and demonstrated close agreement, particularly over land, with a mean difference of $-3\pm11\%$ relative to the MOPITT TIR product.

We use the L2 RPRO v2 product, downloaded from the Non Time Critical (NTC) stream in the Copernicus data space. We only include retrievals with a quality control flag of flag > 0.5 as recommended by Apituley et al. (2024). To allow for a "fair" comparison between the high-resolution TROPOMI retrievals and our coarser $1°\times1°$ transport resolution, we generate $0.5°\times0.5°$ superobservations following Rijsdijk et al. (2025).

2.5.2 Terra-MOPITT

The Measurement of Pollution in the Troposphere (MOPITT) instrument is a gas-correlation radiometer onboard the NASA Terra satellite (Drummond and Mand, 1996). Terra flies a sun-synchronous orbit at 705 km. At nadir, MOPITT has a spatial resolution of about 22 km^2 and overpasses at approximately 10:30 AM and PM local time. Launched already in 1999 (18 December), MOPITT remained active until recently (9 April 2025), delivering a long valuable data record (Canadian Space Agency, 2025). We use the L2 version 9 thermal-infrared (TIR; 4.7 μm band) retrieval product (Deeter et al., 2003, 2022) and exclusively assimilate daytime overpasses. The vertical sensitivity of the MOPITT TIR product (mid-troposphere) is different and complementary to TROPOMI (sensitivity almost uniform throughout the troposphere). The reliability of MOPITT retrievals has been well documented (e.g. Worden et al., 2010; Deeter et al., 2022), with retrieval biases for the version 9 TIR-only data stream estimated to be approximately 5%. The recent implementation of an enhanced cloud detection algorithm in the version 9 product has improved both the coverage and sampling frequency compared to version 8 (Deeter et al., 2022). This particularly benefits regions like the Amazon.

Note that the MOPITT record has a data gap between June 26th and August 24th in 2019 resulting from instrument failure and subsequent decontamination and hot calibration procedures (NCAR, 2024). This period covers substantial CO emissions

https://doi.org/10.5194/egusphere-2025-6213
Preprint. Discussion started: 5 February 2026

according to the bottom-up emissions, which consequently remain unchanged in our inversion when assimilating X_{CO} from MOPITT.

Naus et al. (2022) demonstrated that the TIR product places strong constraints on fire emissions in the Amazon. Alongside the TIR product, MOPITT provides a near-infrared and thermal-infrared (NIR+TIR) product. The NIR product is limited to daytime data and is more sensitive to CO mole fractions in the lower troposphere compared to the TIR product (Deeter et al., 2022). Past CO inversion studies have employed both products, though not simultaneously (e.g. Nechita-Banda et al., 2018; Naus et al., 2022; Peiro et al., 2022).

2.5.3 Ground-based and aircraft observations

The simulations are evaluated against independent in-situ CO measurements from the Atmospheric Tall Tower Observatory (ATTO) site in central Amazonia (Lavric and Walter, 2019). We calculated hourly averages from the 2019 record on the 80 m walk-up tower (2.14°S, 59.00°W). The samples were measured with a Picarro G1302 (CKADS-18) cavity ring-down spectrometer. We converted the data from the WMO X2004 to the WMO X2014A calibration scale. These tower data are used only for evaluation, not assimilation.

We also use aircraft vertical profile measurements from the Obspack collection obspack_multi-species_1_manaus_profiles-_v2.0_2023-09-26 (Miller et al., 2023). The profiles sample the troposphere approximately 80 km north-east of Manaus. In total, nine flights were taken during our study period (22 July - 30 Nov 2019) with descending vertical extents between 5850 m to 250 m (above sea level). The profiles were measured using a Picarro G2401-m (Miller et al., 2023).

We sample TM5 at the location of each individual sample in the tower and aircraft data series using three-dimensional interpolation and hourly averages centred around the measurement time.

2.5.4 Model data mismatch and data selection

The observation error in the cost function usually consists of the actual instrument error (or retrieval/super-observation error) and a representativeness-error estimate of the transport model (i.e. model–data-mismatch error). We determine the latter error contribution following Basu et al. (2018) in which the representativeness error is proportional to the simulated column gradient at a given location with its neighbouring grid boxes. The total model–data mismatch is then taken as the quadratic sum of the instrument and representativeness-error components. To assess whether our assumed error statistics are consistent with the actual model–observation differences, we use the innovation χ^2, defined as:

$$\chi^2_{ino} = \frac{(y - \mathcal{H}(\mathrm{x}))^2}{(HP_t^b H^T + R)} \tag{3}$$

where y is the observation, $\mathcal{H}(\mathrm{x})$ the model equivalent of the observation, P_t^b the prior error covariance and R the observation error covariance or model-data-mismatch. A χ^2_{ino} close to one indicates that the actual residuals are in balance with the expected uncertainties.

https://doi.org/10.5194/egusphere-2025-6213
Preprint. Discussion started: 5 February 2026

The total errors associated with TROPOMI super-observations are generally smaller than the uncertainties that characterise individual MOPITT X_{CO} retrievals ($\sim$3 ppb vs. $\sim$7 ppb on average for all X_{CO}). To ensure that the innovations are neither systematically over- nor under-weighted in the cost function—we increased the model–data-mismatch error by doubling the transport-error component and adding a fixed 4 ppb term. This adjustment reflects our expectation that TM5 has greater difficulty with boundary-layer transport (where TROPOMI is more sensitive than MOPITT) than to free-tropospheric transport (where MOPITT's sensitivity peaks). It also compensates for a likely underestimation of systematic errors in the super-observations and any unaccounted-for error correlations between individual retrievals. After inflation, the mean χ^2_{ino} approached one, indicating a well-balanced and statistically consistent error characterisation.

As our statevector only contains scaling factors for fire emissions, we preselected observations for assimilation. The inversion only considers cases where either the observed or simulated (prior) X_{CO} was recently influenced by fires. We achieve this by applying a condition where either for the observed or modelled $X_{CO} \geq 125$ ppb. We verified that this selection for higher X_{CO} did not result in strong CO accumulation in simulated $X_{CO} < 125$ ppm (Appendix A2) and therefore not bias our fire emission estimates.

Finally, X_{CO} samples with residuals exceeding three times the model–data mismatch (indicative of poor transport model performance in capturing observed fire impacts) are rejected for assimilation. We also exclude X_{CO} samples with reported surface pressure below 900 hPa, as such conditions (e.g. the Andes) are challenging for TM5 to model.

2.6 Inversion procedure

We conducted a series of inversion experiments to quantify Brazilian fire emissions and to assess the robustness of the estimates. These experiments test the sensitivity of the inversion results to the choice of prior fire emission inventory and the assimilated satellite instrument. The different configurations are summarised in Table 2.

In addition to testing the sensitivity to different priors and observational constraints, we quantified how uncertainties in OH chemistry and in CO production from NMVOC oxidation influence the inferred fire emissions. Rather than performing a new suite of inversions, we base this on a set of sensitivity experiments that was targeted to do this for the same region and for four fire seasons, by Naus et al. (2022) (see their Fig. S2). Naus et al. (2022) ran their inversions with two sets of OH fields, and two sets of chemical production fields. For each season that Naus et al. (2022) ran the experiments, we calculate the ensemble standard deviation across their sensitivity experiments and then average these values over all four years. This approach yields an estimated structural uncertainty of 15 Tg CO per season in the posterior fire emissions. We consider this estimate conservative for two reasons: (1) their inversion domain extends beyond Brazil, whereas our reported emissions are limited to the Brazilian portion of the domain, and (2) our system includes an intermediate long-window inversion step.

https://doi.org/10.5194/egusphere-2025-6213
Preprint. Discussion started: 5 February 2026

Table 2. Inversion experiments overview.

Experiment_ID	Fire prior	Assimilated X_{CO}
GFED5.1_TROPOMI	GFED5 .1	TROPOMI
GFASv1.2_TROPOMI	GFAS v1.2	TROPOMI
GFED5.1_MOPITT	GFED5.1	MOPITT

https://doi.org/10.5194/egusphere-2025-6213
Preprint. Discussion started: 5 February 2026

3 Results

3.1 Comparison against observations

In this section, we demonstrate the performance of our inversions by comparing against observations. We start with a comparison to satellite-based X_{CO} and compare to surface observations (in-situ and aircraft). We focus these comparisons on our "base inversion" which started from GFED5.1 and assimilated TROPOMI superobservations.

3.1.1 TROPOMI and MOPITT

The short-window posterior consistently improves agreement with observations compared to the prior. When compared to assimilated TROPOMI data, the simulated and observed X_{CO} compare well, as expected (Fig. 2a - 2f, and Table 3). This improvement is most pronounced for elevated X_{CO} (>125 ppb), where the mean absolute error is reduced by 42–55%, with the strongest error reduction (∼17 ppb) for large X_{CO} (> 225 ppb) that are most representative of fire plumes.

Importantly, this improvement is not limited to assimilated data: validation against independent MOPITT observations also confirm closer alignment between simulated and observed CO (Table 3). The overall improvement in model–data agreement demonstrates that the short-window inversion effectively extracts information from the satellite retrievals.

In terms of spatial structure, the prior residuals are dominated by plume-shaped patterns associated with fire signals (Fig. 2b). The short-window inversion system effectively corrects most biases through adjustments to fire emissions (Fig. 2c). In an exemplary three-day cycle, TROPOMI observations show a plume stretching from north to south on the western flank of the basin (Fig. 2a) that is overestimated or displaced in the prior (Fig. 2b). Furthermore, plume structures south-east of the arc of deforestation are visible, which are strongly underestimated in the prior (Fig. 2b). The inversion corrects much of both discrepancies and substantially reduces biases in plume-dominated regions. Some mismatches remain — for example, the larger than 20 ppb underestimation in the southeastern Cerrado requires emission increases that introduce positive biases at more local scales in the northeastern Cerrado — but overall, the posterior provides the statistically best fit achievable within observational constraints and prior uncertainties.

The inversion also improves the temporal evolution of X_{CO} as confirmed by the Hovmöller diagrams with daily TROPOMI X_{CO} (Fig. 2d-2f). The prior already reproduces broad seasonal variability, but negative biases emerge during the burning season: over the southwestern Cerrado-box (B3), where CO is strongly underestimated from mid-August to October, while the southeastern Amazon-box (B4) shows more rapid variations in the X_{CO} residuals. Note that for both boxes the negative residuals often are synchronous with increases in TROPOMI X_{CO}, indicative of fire episodes. The posterior reduces these residuals throughout most fire episodes.

Table 3 and Figures 2b, 2c, 2e, and 2f (boxes B3, B4) show that in the background-dominated air masses, X_{CO} barely changes and does not deteriorate after the inversion. This shows that our data selection threshold and scaling factor transformation choices did not lead to strong CO accumulation in the background. Together, these outcomes suggest that the short-window prior residual structure is mostly related to fires that the short-window inversion effectively targets by optimising to GFED5.1 bottom-up emissions.

https://doi.org/10.5194/egusphere-2025-6213
Preprint. Discussion started: 5 February 2026

Table 3. Mean absolute error (or residual) and the standard deviation of the residuals per observed X_{CO} bin for the GFED5.1_TROPOMI base inversion.

		MAE ± σ [ppb]			
Range [ppb]	n	Prior		Posterior	
TROPOMI (assimilated)					
0-125	16 613	10	±12	9	±7
125-150	46 357	12	±14	6	±8
150-225	24 465	19	±22	10	±14
>225	1 095	39	±31	22	±27
MOPITT (independent)					
0-125	398 150	8	±10	8	±10
125-150	37 809	15	±16	11	±16
150-225	25 323	24	±26	18	±26
>225	1 139	49	±41	35	±47

https://doi.org/10.5194/egusphere-2025-6213
Preprint. Discussion started: 5 February 2026

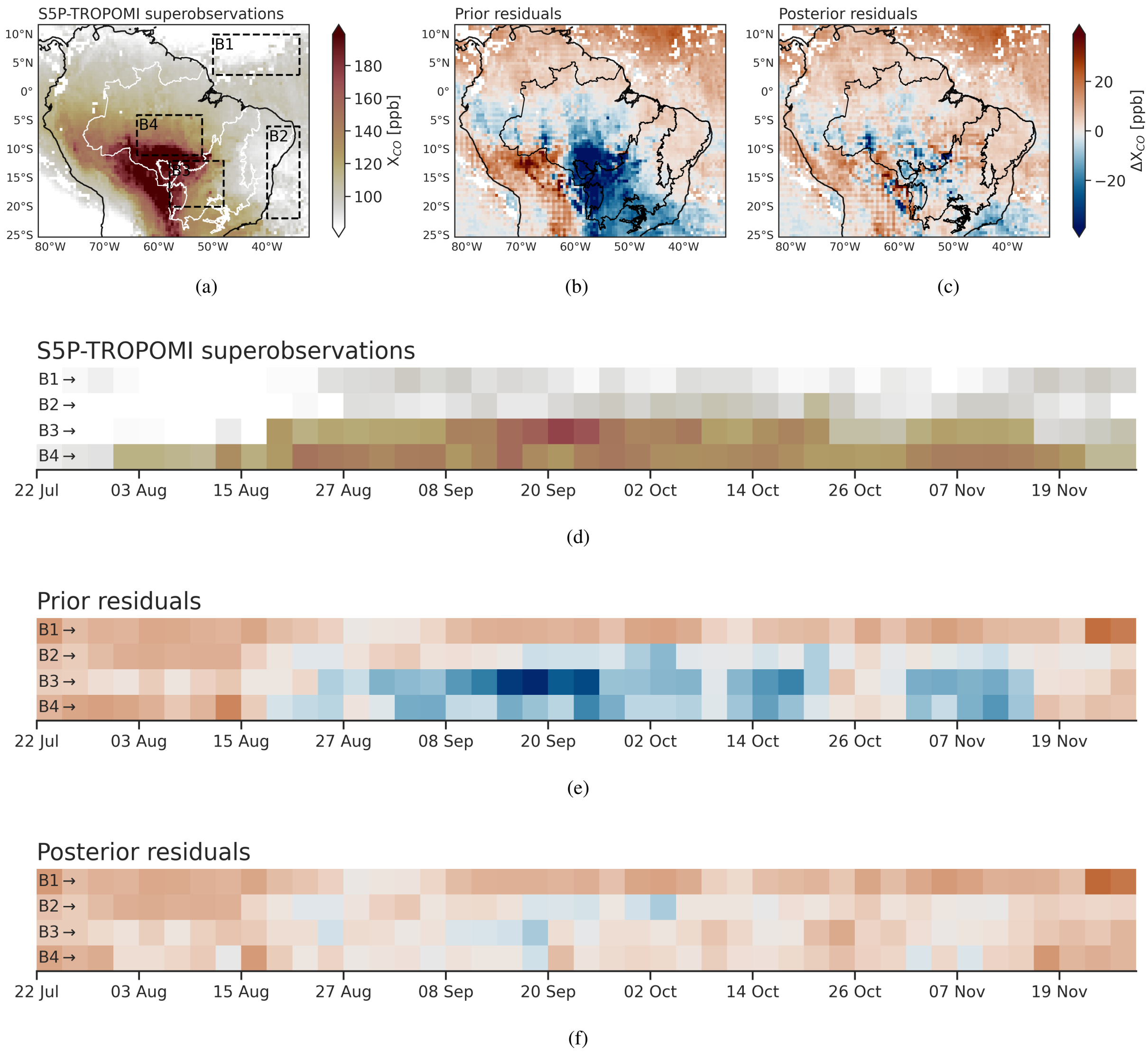

Figure 2. Evaluation of the GFED5.1_TROPOMI base inversion with S5P-TROPOMI superobservations. Spatial maps (a–c) and regional time series (d–f) of X_{CO} and model–observation residuals. (a) TROPOMI X_{CO} averaged to a 0.5°× 0.5°grid for an example 3-day period (14–17 Sep 2019), and corresponding (b) prior and (c) posterior residuals for the same period. (d) Hovmöller diagram of 3-day mean X_{CO} over the subregions indicated in (a): oceanic background (B1, B2), Cerrado (B3), and Amazon (B4); and (e,f) related prior and posterior residuals. Colour bars are shared between (a,d) and (b,c,e,f).

3.1.2 Comparison to in-situ and aircraft observations

While the ATTO measurements do not sample intense fire plumes, they provide valuable independent information to validate background and moderate pollution levels inside the Amazon. Comparison against ATTO CO mole fractions (Fig. 3)

https://doi.org/10.5194/egusphere-2025-6213
Preprint. Discussion started: 5 February 2026

demonstrates that the short-window posterior generally reproduces observed CO mole fractions well, with a mean absolute percentage error of 12% over the 2019 fire season. This level of agreement with independent data provides confidence in the inversions. Note that the difference between the long-window and short-window posteriors reflects the combined changes of increased transport model resolution and fire emission optimisation. The narrow ensemble spread (shading around the lines; nearly invisible), represents the limited sensitivity in both the long- and short-window inversions at this site.

We also evaluate the inversions against independent aircraft CO profiles collected near Manaus (Appendix A3). Compared to the long-window, the short-window inversion provides a clear improvement near the surface in the lower troposphere. The short-window posterior yields a mean absolute percentage error of 19% relative to the observations. Although the short-window tends to better represent the profiles than the long-window inversion, much variability remains across individual profiles. Above 4 km, however, we keep a large positive residual (usually >20 ppb) for all simulations, which we discuss in more detail in Appendix A3.

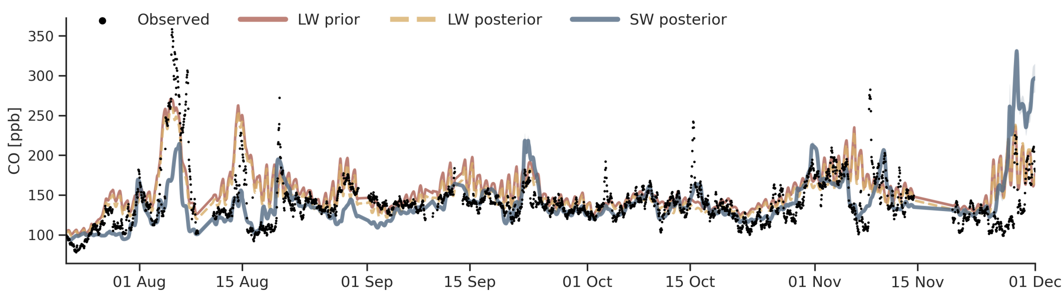

Figure 3. Comparison of measured and simulated CO mole fractions at ATTO at 79 m measurement height (m.a.g.l.). The lines represent the long-window prior (red), long-window posterior (yellow), short-window posterior (blue). Shading around the mean ensemble member show the one standard deviation of the ensemble. The short-window posterior is based on the GFED5.1_TROPOMI inversion.

3.2 Brazilian fire CO emissions during the 2019 fire season

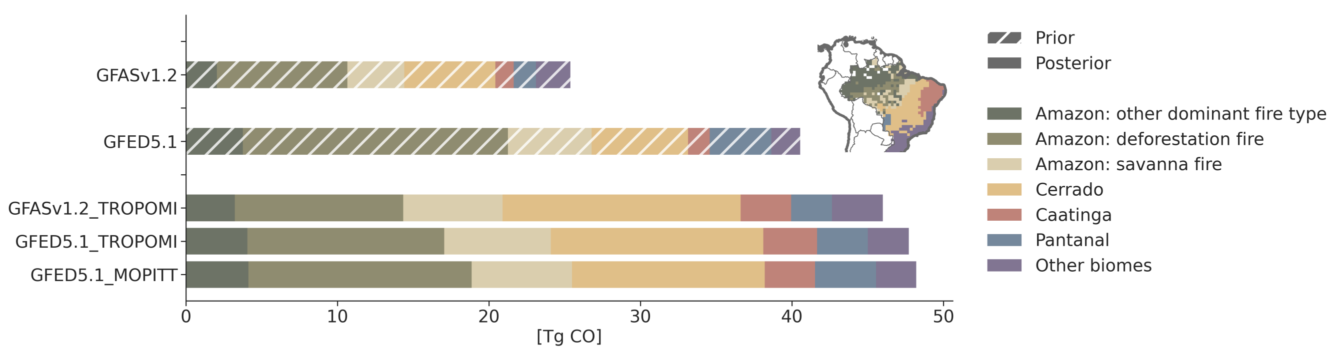

Figure 4. Prior and posterior CO fire emissions [TgCO] for the 2019 Brazilian fire season. Coloured stacked bars represent contributions from different biomes. Emissions in the Amazon biome have been disaggregated to dominant fire types based on Andela et al. (2022).

https://doi.org/10.5194/egusphere-2025-6213
Preprint. Discussion started: 5 February 2026

According to the GFAS v1.2 and GFED5.1 inventories, total CO emissions from fires in Brazil during the 2019 fire season (22 July–30 November) were 25 TgCO and 41 TgCO, respectively, as indicated in Figure 4. Our inversions suggest that fire emissions are 47^{48}_{46} TgCO (mean$^{max}_{min}$). The posterior emissions deviate by less than 20% from the GFED5.1 prior. For GFAS v1.2 however, the inversions imply that an 81% increase of emissions is needed. This prior-posterior increase is substantially higher than the average 50% increase that Naus et al. (2022) found for the 2003-2018 fire seasons and will be discussed in more detail (Sect. 4).

Despite starting from substantially different prior fire-emission totals, the inversions converge to nearly the same posterior fire-emission integral over the season (46.0 TgCO and 47.7 TgCO). Likewise, inversions that assimilate either TROPOMI or MOPITT data end up with similar fire season totals (47.7 TgCO and 48.2 TgCO), underscoring the robustness of the posterior estimates to both the choice of prior and the choice of satellite instrument.

On more local scales (bar-stacks in Fig. 4) or shorter time intervals, the posterior emission spread becomes larger in a relative sense but still demonstrates strong convergence from multiple priors and instruments down to 3-day intervals for most periods analysed (Fig. 5).

3.3 Biome-level fire emissions and their temporal variation

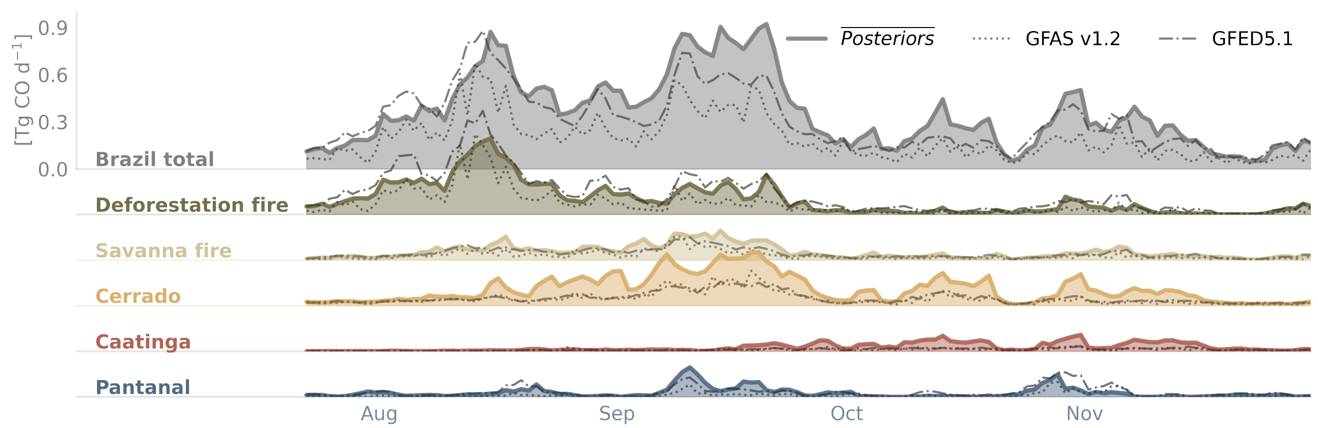

Figure 5. Daily evolution of CO fire emissions by biome. The filled areas and thick lines show the posterior mean of the three inversions (GFED5.1_TROPOMI, GFED5.1_MOPITT, and GFASv1.2_TROPOMI), while the dashed lines indicate the corresponding priors (–.- GFED5.1, ... GFAS v1.2). The posterior spread can be found in Fig. A4.

To better understand the origin and dynamics of posterior–prior differences, we analyse CO emissions at the biome level and their temporal evolution. Given the contrasting fire dynamics and the shifting position of the arc of deforestation relative to biome boundaries, we further subdivided the Amazon emissions into the season's dominant fire types following Andela and Jones (2024). As shown in Figures 4 and 5, savanna fires make a substantial contribution within the Amazon biome (21-32%), and their temporal evolution aligns more closely with Cerrado fires than with deforestation events, supporting this subdivision.

https://doi.org/10.5194/egusphere-2025-6213
Preprint. Discussion started: 5 February 2026

The temporal evolution of fire CO emissions during the 2019 dry season is characterised by a clear succession of different fire regimes (Fig. 5). Both prior and posterior estimates reproduce this phasing, but the posterior estimates highlight important discrepancies in the magnitude of emissions for several biomes—most notably the Caatinga and Cerrado, where optimised emissions differ by a factor of 2–3 from their priors. Figure 5 illustrates this evolution, which we divide into three phases: early-season (mid-August), mid-season (mid-September), and a widespread late-season tail (October-November).

Early season (mid-August)

The early 2019 fire season was dominated by fires in the Amazon biome, with emissions primarily from deforestation and forest fires linked with coarse woody fuels that burn mostly in the smouldering phase. This peak was abnormally early compared to the 15-year preceding GFAS v1.2 and GFED5.1 means (not shown). In this period, priors disagree most: GFAS v1.2 estimates are sometimes up to three times lower than GFED5.1 during the period until late August, adding up to 6.1 TgCO vs. 11.4 TgCO respectively. Meanwhile, the posterior mean estimate falls in between (8.8 TgCO). We note that this period also shows the largest spread in posterior estimates (Fig. A4; adding up to a range of 20.9-25.5 TgCO over the full season). This spread is driven by the absence of observational constraints from MOPITT during most of August (Sect. 2.5.1), while TROPOMI inversions lean towards GFAS v1.2. Furthermore, TROPOMI inversions suggest a minor shift in CO emissions from deforestation to savanna-type fires in the Amazon and Cerrado regions. The mid-august peak in both priors remains preserved, however there seems to be a timing shift of 1-2 days, which may be related to our use of 3-daily (and not daily) scaling factors.

Mid-season (mid-September)

During September, fire activity shifts decisively toward the Cerrado. These fires are characterised mostly by fast-burning, flaming combustion with low CO emission factors (61 gCO/kgDM in GFAS v1.2 and Fig. A5 for GFED5.1). In contrast to the deforestation fires in the early season, the priors are in much closer agreement here. Regardless, the posteriors consistently indicate that an upward adjustment, of often more than two times the prior, is required to agree with MOPITT and TROPOMI observations, reflecting the strongest emission modifications in the inversions. This could suggest that prior inventories underestimate Cerrado fire emissions at the first seasonal peak ($\sim$5 TgCO between mid-August and late September).

Late season (October–November) The late fire season is characterised by a more heterogeneous mix of fire types across multiple biomes. Savanna fires in both the Amazon and Cerrado continue to contribute substantially, accounting for 45% of Brazil's total CO emissions in the prior and increases to roughly 65% in the posterior between October and December. These savanna fires also persist well into late November. From late October onward, some residual burning remains in the Amazon biome, and additional activity emerges in the Pantanal wetlands, which typically requires prolonged dry conditions before they can sustain fire.

During October and November, the posterior mean estimate for Brazil (13.3 Tg CO) indicates that emissions remain considerably higher than suggested by the prior inventories (6.4 Tg CO in GFAS v1.2 and 10.9 Tg CO in GFED5.1), with the most notable increases in the Caatinga and Cerrado regions.

https://doi.org/10.5194/egusphere-2025-6213
Preprint. Discussion started: 5 February 2026

4 Discussion

Our study provides a satellite-constrained estimate of CO fire emissions for the 2019 Brazilian fire season. The convergence of our inversions based on independent X_{CO} from TROPOMI or MOPITT and fire inventories on a total of 46–48 TgCO underscores the robustness of the top-down estimates and highlights the value of satellite instruments to constrain the magnitude of Brazilian fire emissions. This estimate comes with an uncertainty estimate of ~15 TgCO that represents structural knowledge gaps concerning CO production from the oxidation of NMVOCs and loss by OH. Our study also serves as a cross-validation of the two satellite datasets, and the convergence of posteriors shows potential for combined use of the instruments to explore their constraints on the vertical distribution of CO in future research.

4.1 Comparison with prior fire emission inventories

When comparing our inversion results with existing bottom-up inventories, we find encouraging progress in fire emission modelling. This is demonstrated by the good agreement with the new GFED5.1 dataset (posterior within <20% of GFED5.1), as opposed to the older GFAS v1.2 product (posterior deviates >80%). The agreement with GFED5.1 suggests that recent updates, such as the inclusion of the new small-fire burned area dataset, help to better capture regional fire regimes.

When analysed at biome level, the inversion suggests large fire emission changes for fires in the Amazon, ranging between 3-9 TgCO, with a reduction and increment compared to GFED5.1 and GFAS v1.2 respectively. However, the posterior mean (23.5 TgCO) ends up well within the large prior range of 14.3-26.8 TgCO as inventories in tropical forest regions remain uncertain. Detection of emissions from understory fires remains inherently challenging due to persistent cloud cover and dense canopies (Morton et al., 2013). It should be acknowledged that our posterior spread remains relatively large for this region (20.9-25.5 TgCO) in part due to limited observational constraints from MOPITT during the peak of the fire season here and that our system has limited capacity to account for a lack of emissions due to missed detections, as will be discussed later.

In contrast, we find systematic emission increments for the Cerrado and the Caatinga biomes. The inversion adjusts the prior by a factor two, resulting in a 7-8 TgCO prior-posterior gap. This result is unexpected, as fire dynamics in these savanna-dominated ecosystems are typically considered relatively well captured and constrained by global inventories due to availability of ground measurements and relatively straightforward fire dynamics. Our findings however, are in line with previous work by Naus et al. (2022), who also reported a systematic underestimation of savanna and shrubland fire emissions by GFAS v1.2. In their work the median difference between the prior and posterior emissions also approached a factor of two, while using a different inversion algorithm (4D-var v. EnKF), meteorological driver data (ERA-Interim v. ERA5), and different CO source/sink datasets. The remainder of this discussion will investigate the potential drivers of this large and systematic discrepancy between our inverse results and the fire inventories..

4.2 Potential drivers of the Cerrado/Caatinga emission gap

To understand the source of the discrepancy between the prior and posterior Cerrado/Caatinga emissions, we first assess potential errors in our inversion framework before discussing the prior inventories.

https://doi.org/10.5194/egusphere-2025-6213
Preprint. Discussion started: 5 February 2026

First, transport modelling errors can play a role. The comparison of TM5 simulated vertical profiles of CO against observed CO from aircraft flights near Manaus suggest that convective mixing of surface signals aloft is too strong in TM5 (Fig. A2). At the same time, major errors in vertical transport seem unlikely given the strong consistency between TROPOMI- and MOPITT-based inversions despite their different vertical sensitivities and overpass times. Nonetheless, transport modelling errors remain a source of uncertainty in atmospheric inversions. These uncertainties are challenging to quantify and would benefit from for instance an inter-comparison study with different transport models over South America, which is beyond the scope of this work.

Second, Lichtig et al. (2024) showed that African fires contribute up to 25% of tropospheric CO mass over eastern Brazil. The good agreement between TROPOMI observations and TM5 simulated fields over the main inflow regions (Sect. 3.1.1, Fig. 2d) suggest however that long-range transport biases are small. Moreover, the good agreement negates the hypothesis that the high emissions are a compensation for a lack of CO inflow from distant fire emissions or CO production from CH_4 oxidation in the background atmosphere.

Third, localised chemical sources or sinks – such as CO production from NMVOC oxidation or loss through OH – remain an alternative explanation for the differences over the Cerrado and Caatinga. However, the magnitude of the sub-regional changes required makes this unlikely. To close the emission gap, NMVOC-derived CO production in these regions would need to increase two- to fourfold. Besides, this assumes a 1:1 compensation between NMVOC-CO and fire-CO, but as Naus et al. (2022) demonstrated, the relationship is closer to 2:1, implying an even larger and less plausible adjustment would be needed. Furthermore, such a large, localised change in the NMVOC source would require compensating biases elsewhere and degrade the current good agreement with independent CO budget estimates (Zheng et al., 2019; Naus et al., 2022).

Following the same reasoning, we think that large OH biases in the Cerrado/Caatinga are improbable. Moreover, the CAMS state-of-the-art chemical data assimilation system has constraints on species important for OH-chemistry through extensive assimilation of satellite observations, making such systematic biases in our imposed OH fields unlikely. Also, a recent inter-comparison by Jones et al. (2025) shows that CAMS EAC4 surface ozone (a key OH precursor) lies at the low end of current reanalyses, suggesting that EAC4 could more likely underestimate than overestimate OH. More OH in our inversion would, if anything, increase inferred fire emissions, further stretching the prior-posterior Cerrado/Caatinga emission gap.

While structural uncertainties in the representation of the chemical sources and sinks are substantial, $\pm$15 TgCO (see Section 2.6), we argue that the current chemical source and sink terms cannot fully account for the Cerrado/Caatinga posterior estimates without degrading agreement with observations in downwind regions (e.g. Section 3.1.1). Therefore, the adjustment in the Cerrado/Caatinga seems to be plausible not only because it is independent of the data assimilated in our inversions, but also because it is consistent with other top-down studies that found larger CO and CO_2 emissions in the Cerrado and Caatinga biomes (Naus et al., 2022; Botía et al., 2025).

4.2.1 Global fire emission inventory perspective

In previous research, underestimation of fire emissions has often been linked to missing small fires (Ramo et al., 2021; Roteta et al., 2019; Randerson et al., 2012). These are, however, now accounted for in GFED5.1 (Chen et al., 2023; van der Werf

https://doi.org/10.5194/egusphere-2025-6213
Preprint. Discussion started: 5 February 2026

et al., 2025). Compared to the Amazon, the savannas of the Cerrado and Caatinga usually have less cloud cover and lower canopy density, which facilitates more reliable satellite-based fire detections. For these reasons, we expect undetected fires to contribute only marginally to the remaining prior-posterior discrepancy.

Second, uncertainties in CO emission factors (EFs) could contribute to the emission gap, but it is unlikely that they can explain the mismatch between bottom-up inventories and our top-down study entirely. Literature reported uncertainties in CO EFs for savanna fires are 28-30% (Andreae and Merlet, 2001; Andreae, 2019) and the Cerrado/Caatinga average CO EFs in GFAS v1.2 and GFED5.1 are substantially different, with 65 g CO/kg dry matter in GFAS v1.2 (Kaiser et al., 2012; Andreae and Merlet, 2001), while GFED5.1 approaches a region weighted average of 55 g CO/kg dry matter when the majority of dry matter is combusted (Fig. A5). Taking this into consideration, a 20% uncertainty in the prior EF appears reasonable. However, applying a 20% increase to the prior emissions would only account for about 20% of the ∼8 TgCO prior-posterior Cerrado/Caatinga emission gap. To close the gap entirely, the average EF for these savanna fires would need to exceed that of tropical forest fires (101-109 g CO/kg dry matter (Andreae and Merlet, 2001; Andreae, 2019)), which is unrealistically high for savanna fires. Therefore, while EF uncertainties may be a contributing factor, they alone cannot resolve the factor-of-two discrepancy between our posterior estimates and the prior inventories.

A third possible source of underestimation lies in how the two inventories calculate total matter burned. Although GFAS v1.2 and GFED5.1 report similar total CO emissions for the Cerrado/Caatinga (7.2 and 7.8 TgCO, respectively), their substantially different CO EFs imply that their underlying total dry matter burned estimates are not in agreement. For GFAS v1.2, Eames et al. (2025) also found (total carbon) emissions to be on the low end for a savanna region in Africa and listed three potential reasons related to underestimated total matter burned that are relevant for the Cerrado/Caatinga region too: A) GFAS is tuned to the older GFED (version 3) version that did not account for small fires, B) use of a globally unified conversion factor from FRE to mass DM burned (kgDM MJ^{-1}) that may not be representative for all savanna types, and C) weakening of the FRE signal by tree canopies in woody savannas.

Recent studies also support the hypothesis of underestimated fuel loads in GFED5.1. Forkel et al. (2025) demonstrated that the woody debris and litter estimates in GFED500m (Van Wees et al., 2022) are low for the Cerrado when compared to both field measurements and a GEDI LiDAR-based fuel map from Leite et al. (2022). This is particularly important because litter and coarse woody debris constitute over 90% of the fuel in savanna fires within the Amazon and Cerrado biomes according to Forkel et al. (2025), underscoring the need for accurate characterisation of these fuel pools. Even minor shifts in fuel quantity can be significant if they coincide with shifts towards fuel types associated with higher CO EFs.

Accurate modelling of these fuel pools at a global scale remains a major challenge. As both Van Wees et al. (2022) and Eames et al. (2025) discuss, surface and below-canopy fuels are difficult to observe with satellites. Consequently, models often rely on empirical tuning. For instance, the GFED model's carbon pool turnover rates are tuned using data from field campaigns (Van Wees et al., 2022), which may not capture the full heterogeneity of the vast and diverse Cerrado/Caatinga region.

Finally, fire dynamics over the regions have been changing and it is unclear if global inventories represent this well. Our inversion indicates the largest emission adjustments in the northeastern Cerrado (MATOPIBA: Maranhão, Tocantins, Piauí, and Bahia) region, an area where most native vegetation remains, which are under strong pressure from human activities (Silva

https://doi.org/10.5194/egusphere-2025-6213
Preprint. Discussion started: 5 February 2026

et al., 2021; Alencar et al., 2020). Over the past three decades, nearly half of the Cerrado's native vegetation has been converted to other land uses (Alencar et al., 2020), which could imply fundamental alterations in fire characteristics such as fuel type, load, and consumption, and consequently, emission factors that may not be adequately included in global inventories. While the years pre- and post land use conversion show increased fire activity, negative trends in burned area emerge as the converted lands age (Ribeiro et al., 2024). Human activities fragment the landscape, which can disrupt the natural cycle of frequent, low-intensity fires, leading to woody encroachment (Stevens et al., 2017; Rosan et al., 2019). This build-up of fuel increases the risk of larger and more intense fires (Fidelis et al., 2018). More woody fuels in turn usually are characterised by higher EFs. For example, provided that emission factors in inventories often are (at least in part) based on field measurements before the 2000's and static in time (e.g. Kaiser et al., 2012; Andreae and Merlet, 2001), such dynamics may not be represented through emissions factors.

4.3 Outlook and Future Directions

This study and our new modelling framework open the path for future research. For example, we want to highlight the potential of leveraging CO to improve fire detection and quantification, particularly for small and cloud-obscured fires that traditional bottom-up methods may still under-represent. Although our current framework effectively constrains regional emissions, it has only limited capability to assign emissions locations where the priors have no or low emissions because the errors we assign to each location depends on the magnitude of the local fire emission itself. Future studies could build on our work by implementing more flexible prior error structures. For example, adopting approaches that allow the inversion to allocate emissions more freely, such as in Yin et al. (2015), could allow a more complete exploitation of downwind CO observations and refine emission estimates for low-intensity fire regimes.

Furthermore, our data selection strategy focused on fresh fire plumes by using a 125 ppb threshold, which proved effective in constraining peak fire emissions without introducing strong biases in CO background mole fractions. Future work should explore more dynamic data selection methods or consider assimilation of background X_{CO} in the long-window inversion step. Such advancements would allow for the assimilation of all available observations, which could help to capture more diffuse, widespread fire emissions that lead to lower yet detectable X_{CO} increases.

Ultimately, our goal is to accurately quantify total carbon release. We convert the CO emissions to total carbon using pre-determined $\frac{CO}{CO_2}$ ratios, as done in previous studies (e.g. Gatti et al., 2010; van der Laan-Luijkx et al., 2015; Peiro et al., 2022; Basso et al., 2023; Bowman et al., 2017; Byrne et al., 2024; van der Velde et al., 2021b; Koren, 2020; Botía et al., 2025). Assuming the prior $\frac{CO}{CO_2}$ ratios, our posterior CO estimates translate to fire carbon emissions of 270–278 TgC for the 2019 Brazilian fires, compared to 141-205 TgC according GFAS v1.2 and GFED5.1 respectively. This is roughly 100 TgC larger than previous estimates (Andela et al., 2022). Roughly 50–70% of this prior-to-posterior increase stems from the Cerrado and Caatinga. This not only highlights the importance of savanna fire carbon emissions but also the critical uncertainty in $\frac{CO}{CO_2}$ emission ratios. Future work would benefit from further investigation of the $\frac{CO}{CO_2}$ emission factor ratios, and potential constraints thereon. For instance, joint CO/CO_2 inversions would allow the co-optimisation of the emission ratios using alternative combustion efficiency proxies like $\frac{\Delta X_{NO_2}}{\Delta X_{CO}}$ from (van der Velde et al., 2021a).

https://doi.org/10.5194/egusphere-2025-6213
Preprint. Discussion started: 5 February 2026

5 Conclusions

We introduced the new CTE-LW/SW atmospheric inversion framework for CO to provide complementary satellite-based constraints on fire emission inventories and applied it to the 2019 Brazilian fire season. By assimilating X_{CO} data from both TROPOMI and MOPITT, we derive a top-down estimate of 46-48 TgCO for this period. A limitation is that we made this estimate using a single representation of non-fire CO sources and sinks. Uncertainty in these terms, presumably driven by CO production from NMVOC oxidation and loss via OH oxidation, could systematically bias inferred fire emissions; sensitivity tests indicate a structural uncertainty of $\sim$15 Tg CO. The strong convergence between inversions using different satellite instruments and prior inventories (GFED5.1, GFAS v1.2) nonetheless demonstrates robustness and simultaneously functions as independent cross-validation of these key satellite datasets over a complex, fire-dominated region.

At the national scale, our posterior emissions agree within <20% with the new GFED5.1 inventory, which signals progress in bottom-up fire emission modelling. Nonetheless, at the biome-level, we surprisingly find that emissions from the Cerrado and Caatinga biomes are nearly twice as large as the inventories. This systematic underestimation in savanna and shrubland ecosystems, consistent with previous studies, points to unresolved challenges in top-down and/or bottom-up emission modelling. Understanding this mismatch is important for carbon budgeting, because relatively low $\frac{CO}{CO_2}$ emission factor ratios, on which the use of CO as a proxy for total carbon usually relies, implies that these fires, would have relatively strong implications for total carbon emissions.

Our findings underscore the value of X_{CO}-based atmospheric inversions for monitoring fire emissions and evaluating emission inventories in fire-prone regions. More broadly, this work helps to advance our understanding of the carbon impacts of (extreme) fire events in Brazil and provides a framework to support improved mitigation, monitoring, and policy-relevant assessments of fire-driven carbon fluxes.

https://doi.org/10.5194/egusphere-2025-6213
Preprint. Discussion started: 5 February 2026

Code and data availability. The CTDAS and TM5-MP living codebases are openly accessible at https://git.wur.nl/ctdas and https://ci.tno.nl/gitlab/tm5/tm5-mp, respectively. The posterior daily gridded CO fire emissions from this study along with the CTDAS inversion and TM5-MP transport model code versions used to generate these posterior emissions, are archived at https://doi.org/10.5281/zenodo.17881656 (van den Berg, 2025)

https://doi.org/10.5194/egusphere-2025-6213
Preprint. Discussion started: 5 February 2026

A1 Long-window CO inversion

We performed a six-year (2014–2020) long-window atmospheric CO inversion to obtain a CO budget that is consistent with observed CO concentrations. This optimised atmospheric state and budget then serve as the initial conditions for the short-window inversion. An overview of the CO long-window configuration is provided in Table A1. In this configuration, fire emissions are prescribed. To minimise the aliasing of fire signals onto other sources, we assimilate only observations with no or very weak fire influence and apply coarse, tightly constrained scaling factors to the budget components.

For details on the design philosophy of the long-window/short-window inversion framework, as well as a demonstration of the system for CO_2, we refer to van der Woude (2024).

Prior chemical CO production fields from NMVOC and CH_4 oxidation for the long-window inversion are taken from a TM5-MP chemistry run with extended hydrocarbon chemistry for 2018, following Myriokefalitakis et al. (2020). In this dataset OH was reported to be too high, which led to overcompensation in the chemical CO production terms. To avoid a strongly biased start-conditions, we pre-scaled the NMVOC and CH_4 fields. Additionally, to represent known inter-annual variability in the CH_4, we scaled the CH_4 oxidation fields to the CH_4 atmospheric growth rate from NOAA (Lan et al., 2022).

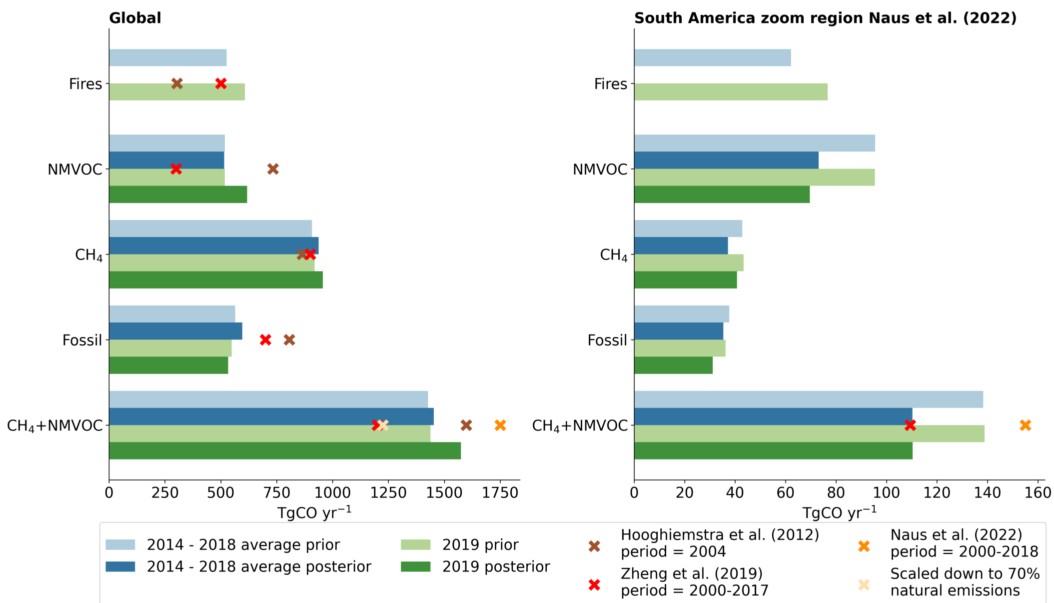

Figure A1. Long-window inversion CO budget overview. Note that the zoom region in Naus et al. (2022) spans from 75 to 39°W and from 28°S to 8°N.

https://doi.org/10.5194/egusphere-2025-6213
Preprint. Discussion started: 5 February 2026

Table A1. Long-window CO inversion configuration.

Statevector		$\lambda_{r,t}^{\mathrm{NMVOC}}$	$\lambda_{r,t}^{\mathrm{CH_4}}$	$\lambda^{\mathrm{ant}_{r,t}}$
Spatial structure (r)		5° latitude bands	5° latitude bands	TRANSCOM regions
Update frequency (t)		monthly	monthly	monthly
Correlation length[1]	[km]	1000	1000	None
	[months]	3	3	4
Inter-yearly correlation[1]	[T/F]	T	T	T
	[years]	3	3	3
Prior uncertainty	[%]	7%	7%	5.5%
Prior dataset		0.55×TM5 full chemistry fields (Myriokefalitakis et al., 2020)	0.80×TM5 full chemistry fields (Myriokefalitakis et al., 2020)	CAMS GLOB ANT v6.2 (Granier et al., 2019; Soulie et al., 2024)

Other	
Assimilated observations	Flask samples from obspack_co_1_GLOBALVIEWplus_v4.0_2024-02-13 with no assimilation concerns (Schuldt et al., 2024)
Model data mismatch	5.5 ppb
Initial CO concentrations	CAMS EAC4 (Copernicus Atmosphere Monitoring Service, 2020; Inness et al., 2019)
Tropospheric OH	CAMS EAC4 (Copernicus Atmosphere Monitoring Service, 2020; Inness et al., 2019)
Stratospheric OH	Climatology (Brühl and Crutzen, 1993)

[1] This represents the correlation distance or time after which the correlation strength decays by a factor of e.

A2 Data selection and scaling factor transformation

We applied a condition (observed X_{CO} $>=$ 125 ppb | simulated (cycle prior) X_{CO} $>=$ 125 ppb) for selecting X_{CO} to assimilate and a scaling factor transformation to avoid negative posterior emissions. By including the "or simulated X_{CO}" criteria, we make sure that the inversion has freedom to scale down a fire when it is modelled in the short-window prior but not observed.

In Table A2, as well as the independent MOPITT X_{CO} $<$ 125 ppb in Table A2, provide evidence that these decisions did not or not strongly degrade the simulated columns for the lowest bin. It shows that the simulated "background" retrievals did not result in systematically overestimated "background" columns.

https://doi.org/10.5194/egusphere-2025-6213
Preprint. Discussion started: 5 February 2026

Table A2. Mean absolute error (or residual) and the standard deviation of the residuals per observed X_{CO} bin. Extension of Table 3 with the subset of TROPOMI X_{CO} that was rejected for assimilation by the (observed $X_{CO} > 125$ ppb | simulated (cycle prior) $X_{CO} > 125$ ppb) criteria.

	MAE $\pm\,\sigma$ [ppb]		
Range [ppb]	n	Prior	Posterior
TROPOMI (not-selected for assimilation)			
0-125	497 780	6 ±8	7 ±7

A3 Comparison against vertical profiles near Manaus

The TM5 simulations reproduce the observed vertical CO profiles over Manaus reasonably well (Fig. A2). Across the nine flights, the short-window posterior yields a mean absolute percentage error of 19%, consistent with the the ATTO tower evaluation (Fig. 3). In the lower troposphere, the short-window posterior (blue) generally aligns more closely with the observations than the long-window posterior (orange). This improvement is driven primarily by the higher transport resolution (6°×4° versus 1°×1°) and, to a lesser extent, by sensitivity to fire emissions within 3 days of the profile measurements.

In a few cases (28 July, 11 August, and 5 November), we detect limited (lower-)profile sensitivity to prior fire emissions in the short-window inversion (not shown). For these dates, the differences between the long- and short-window posteriors in the lower half of the profiles are consistent with reductions in upwind tropical forest fire emissions around that period (see, e.g., Fig. 5). However, because the aircraft did not sample intense, freshly lofted smoke plumes, this comparison remains inconclusive for evaluating short-window performance. To fairly evaluate the short-window performance, targeted in-plume measurements would be critical.

Fig. A2 also demonstrates that even when observed profiles suggest substantial fire contributions (e.g. 11 Aug), an improved model–observation match is not guaranteed. We attribute this partly to the spatial error correlations imposed in the inversion, which distribute emission adjustments across a broader upwind region rather than allowing independent changes at the grid-cell level. Additionally, emissions are optimised over 3-day windows rather than daily, limiting the system's ability to capture highly localised plume peaks. These results only underscore a fundamental characteristic, namely that atmospheric inversions such as ours are not designed to constrain super-local, day-specific plumes.

The Manaus profile comparison show that the long-window inversion exerts only a minor influence on CO levels over the Amazon (typically <10 ppb). Because we did not assimilate local flask observations, the long-window inversion is effectively insensitive to the sub-regional variability captured in the lower half of the aircraft profiles. In addition, the current long-window configuration was intentionally configured to adjust only large-scale, slowly varying components of the global CO budget which restricts the inversion's freedom to constrain such local fluxes in central Amazonia. As a result of these choices, we find the long-window prior ensemble spread is narrow and the posterior remains close to the prior in the Manaus profiles.

A persistent positive residual that averages around 20 ppb remains in the free troposphere of the simulated profiles. The bias reflects, at least in part, large-scale transport or flux errors. This is demonstrated by Fig. A3, which shows long-window

https://doi.org/10.5194/egusphere-2025-6213
Preprint. Discussion started: 5 February 2026

posterior residuals of similar magnitude at Farol de Mae Luiza (NAT)—and at times also at Ascension Island (ASC)—during July–December 2019. These locations frequently influence free tropospheric air masses near Manaus during this period of the year. Nonetheless, NAT and ASC remain surface sites and may therefore not capture potential unresolved biases in CO fluxes that originate from the African mainland to their full extent. As a consequence, we cannot conclusively determine how much potential large-scale transport or flux errors contribute to the free-tropospheric residuals observed over Manaus.

Alternatively, the residual could reflect local-scale flux errors and/or in vertical mixing/boundary-layer venting. Previous studies have identified TM5 as fast-mixing compared to other chemistry transport models (Krol et al., 2018; Jin et al., 2025; Remaud et al., 2023). The frequent lack of steepness in the simulated profile vertical gradients are indeed indicative of too much (deep convective) vertical mixing. However, we consider major vertical mixing biases for our full domain and study period unlikely for two reasons: (1) excessive upward mixing would also require low CO in the boundary layer—especially in the unoptimised long-window prior—which is not (systematically) evident from the Manaus profile comparison; and (2) substantial vertical mixing errors would be expected to produce inconsistent short-window results between the MOPITT and TROPOMI driven inversions, given their different averaging-kernel structures. Instead, we find highly consistent solutions. Although this does not necessarily confirm that TM5 does not have any vertical-mixing issues, it does demonstrate that it unlikely presents itself as dominant driver of the free-tropospheric residual.

https://doi.org/10.5194/egusphere-2025-6213
Preprint. Discussion started: 5 February 2026

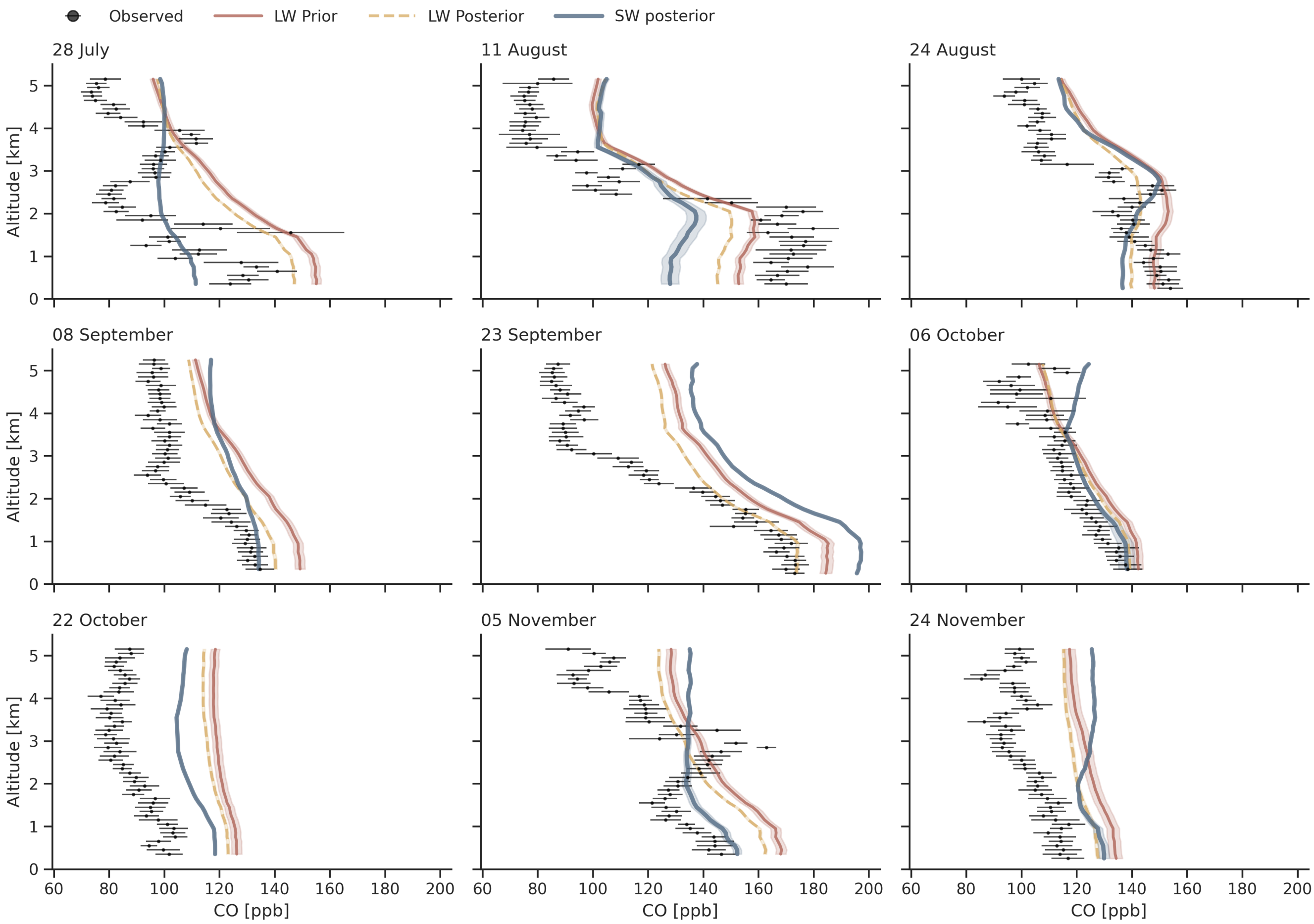

Figure A2. Comparison of measured and simulated carbon monoxide (CO) vertical profiles from nine research aircraft flights near Manaus (2.595°S, 60.209°W), each containing approximately 50 individual measurements (total = 455). Coloured lines show the ensemble mean of the simulated profiles (150 ensemble members for both inversions), and shaded regions indicate the ensemble standard deviation. The short-window posterior results are derived from the GFED5.1_TROPOMI inversion. Black points represent observed profiles with each point representing a time interval average (median length of 42-seconds and 42 samples per interval); error bars denote the corresponding standard deviation.

https://doi.org/10.5194/egusphere-2025-6213
Preprint. Discussion started: 5 February 2026

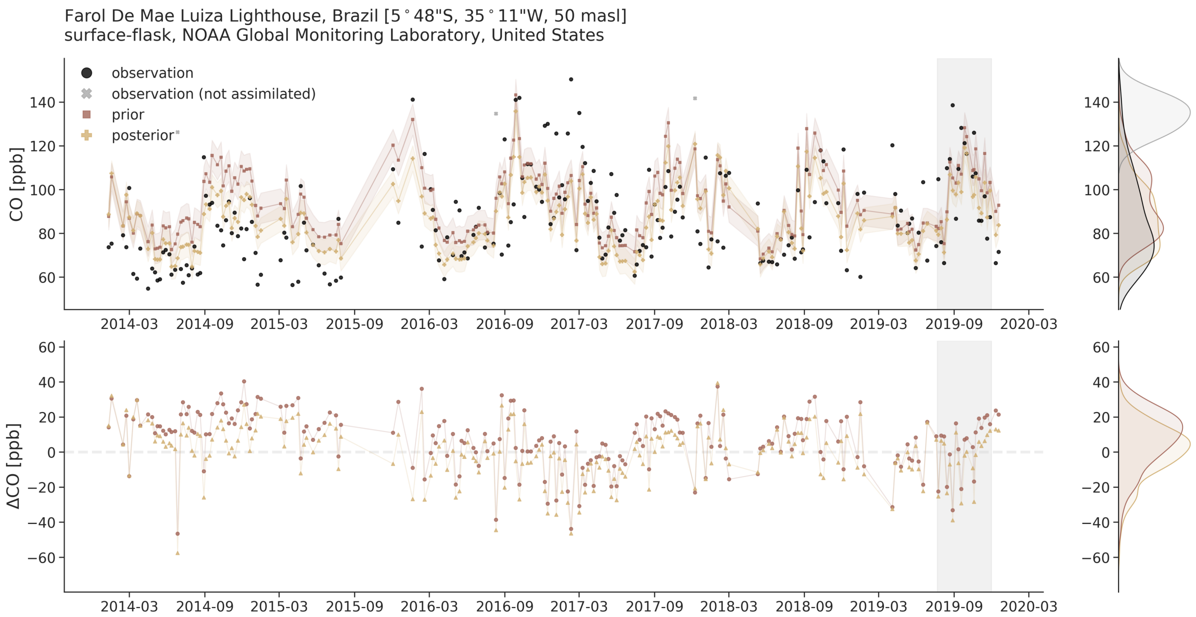

(a)

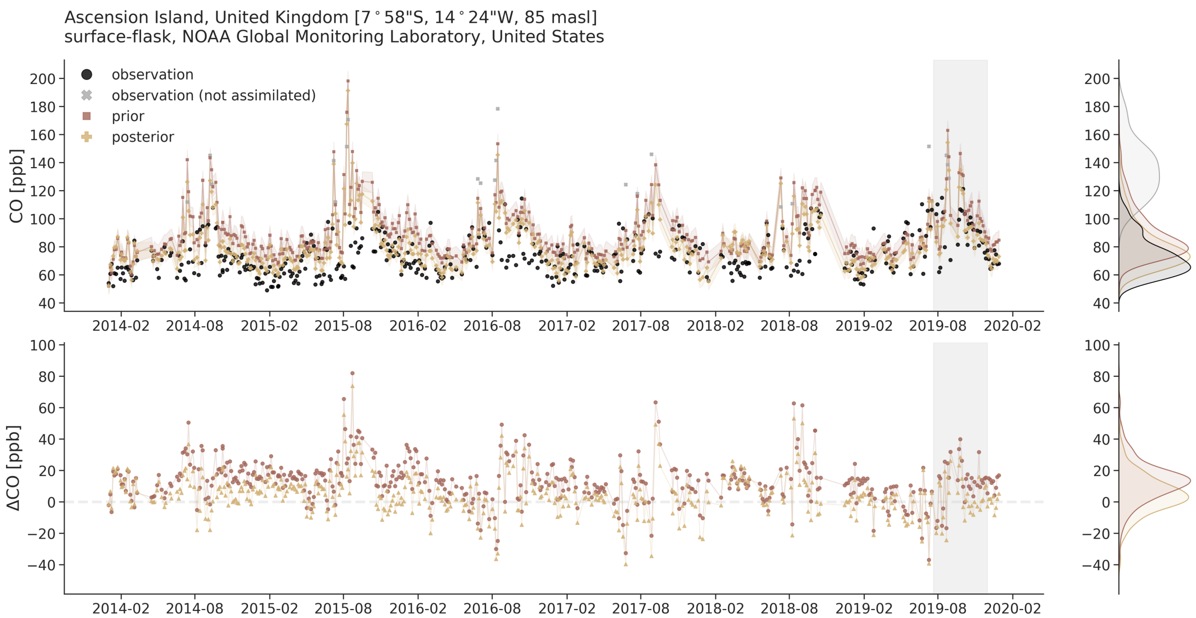

(b)

Figure A3. Comparison of observed (black/gray) and simulated CO mole fractions at ASC and NAT from the long-window inversion. Prior simulations are shown in red and posterior simulations in yellow. Shaded areas represent one standard deviation away from the ensemble mean together with the model–data mismatch. Top panels show CO mole fractions, bottom panels show residuals (model – observation), both with corresponding distributions on the right. The grey shaded box indicates the short-window simulation period.

https://doi.org/10.5194/egusphere-2025-6213
Preprint. Discussion started: 5 February 2026

A4 Posterior spread in fire emissions

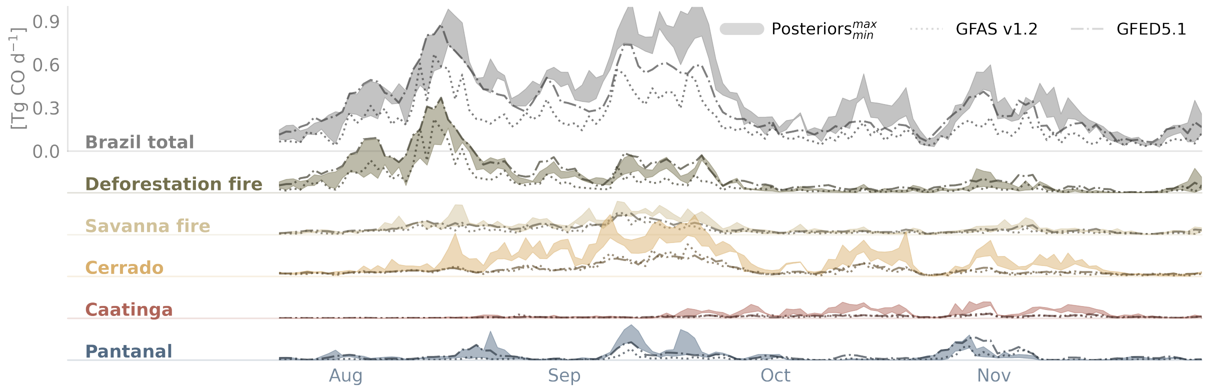

Figure A4. Same as Fig. 5 in the main text, but with the shaded area showing the full posterior range (minimum to maximum) instead of the posterior mean.

585 The posterior spread is generally is small and tends to fall outside the prior-range for Cerrado, Caatinga and Amazon-biome-savanna fires. The only notable exception is early on in the season for deforestation fires. While the TROPOMI inversions there tend to scale towards the GFAS v1.2 emissions, the GFED5.1_MOPITT inversions lacks constraints due to the 1-month instrument outage (Section 2.5.1). This presumably is resulting in the large posterior spread, while later on in September with active MOPITT constraints the posterior spread reduced rapidly even though the prior spread was very large there.

590 ## A5 Emission factors

Figure A5 illustrates the general behaviour of CO emission factors (EFs) for savanna fires in the Cerrado/Caatinga savannas, as represented in GFED5.1 . The figure shows that the daily, dry-matter-weighted CO EF (blue line) is dynamic, fluctuating throughout the year. Early in the season, during more humid conditions, the EFs are higher. During the peak fire season (August-October), when fuels are dry, the vast majority of dry matter is combusted (green area) and average EF decreases to
595 approximately 55-58 g CO/kg dry matter. This is substantially lower than the static EF of 63 g CO/kg dry matter used in the previous GFED 4 inventory (red line). Later in the season the EF increases again; Vernooij et al. (2023) hypothesise that this reflects an increased contribution from woody fuels that become dry enough to burn.

https://doi.org/10.5194/egusphere-2025-6213
Preprint. Discussion started: 5 February 2026

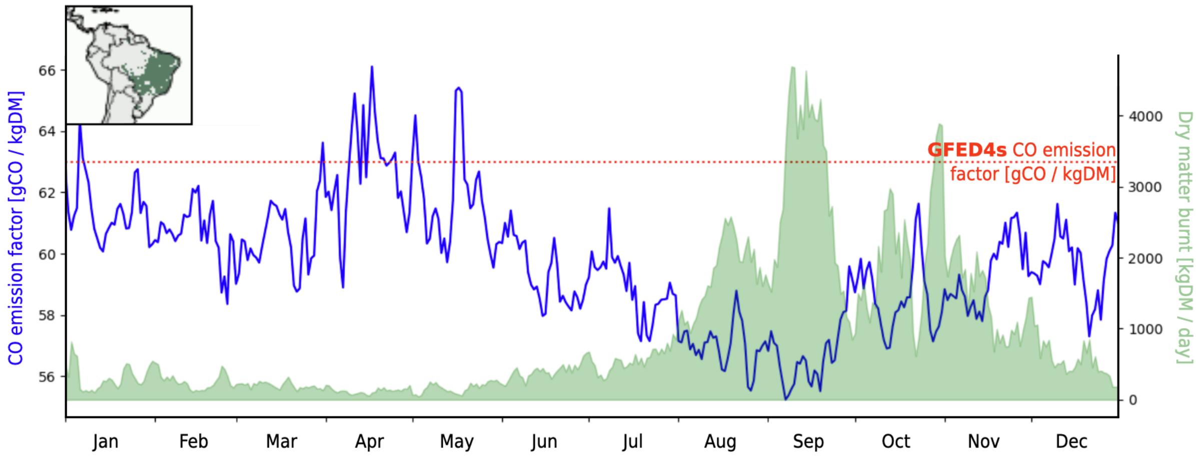

Figure A5. Seasonality of the savanna CO emission factors (EF; blue; left axis) averaged over the region indicated in the inset panel from GFED5.1 (the EFs are weighted by dry matter). The green shaded area shows the region total kg dry matter (DM; right axis). The red line indicated the fixed emission factor that was previously used in GFED 4.

https://doi.org/10.5194/egusphere-2025-6213
Preprint. Discussion started: 5 February 2026

Author contributions. AB, MK, and WP designed the study. JH and AB performed the long-window inversion and analysis. AB performed the short-window inversion and analysis with contributions from WP, MK, IL, JD, and AW. PR provided software for the superobservations. GW and RV provided GFED data. JM provided the Manaus profiles. AB wrote the paper with contributions from all co-authors.

Competing interests. The contact author has declared that the authors do not have any competing interests

Acknowledgements. We would like to thank J. V. Lavric and D. Walter for conducting and sharing the ATTO CO measurements. We thank the Instituto Nacional de Pesquisas da Amazonia (INPA) and the Max Planck Society for continuous support. We acknowledge the support by the German Federal Ministry of Education and Research (BMBF contracts 01LB1001A and 01LK1602B) and the Brazilian Ministério da Ciência, Tecnologia e Inovação (MCTI/FINEP contract 01.11.01248.00) as well as the Amazon State University (UEA), FAPEAM, LBA/INPA and SDS/CEUC/RDS-Uatumã. We would like to thank R.A.F. de Souza and G. A. Martins for co-organising and sharing the CO profile measurements near Manaus. This project has received funding from the European Union's Horizon 2020 research and innovation programme under Grant Agreement No. 958927 and 101082194. The simulations are carried out on the Dutch national e-infrastructure with the support of the SURF Cooperative and funding from the Nederlandse Organisatie voor Wetenschappelijk Onderzoek (grant no. NWO-2025.010). ChatGPT was used as language editor to help improve the readability of parts of this manuscript and the AI tool Copilot for debugging and scripting purposes, the results and content of which was always checked and reviewed by the authors.

References

Alencar, A., Nepstad, D., and Diaz, M. C. V.: Forest Understory Fire in the Brazilian Amazon in ENSO and Non-ENSO Years: Area Burned and Committed Carbon Emissions, Earth Interactions, https://doi.org/10.1175/EI150.1, 2006.

Alencar, A., Z. Shimbo, J., Lenti, F., Balzani Marques, C., Zimbres, B., Rosa, M., Arruda, V., Castro, I., Fernandes Márcico Ribeiro, J. P., Varela, V., Alencar, I., Piontekowski, V., Ribeiro, V., M. C. Bustamante, M., Eyji Sano, E., and Barroso, M.: Mapping Three Decades of Changes in the Brazilian Savanna Native Vegetation Using Landsat Data Processed in the Google Earth Engine Platform, Remote Sensing, 12, 924, https://doi.org/10.3390/rs12060924, 2020.

Alencar, A. A. C., Solórzano, L. A., and Nepstad, D. C.: Modeling Forest Understory Fires in an Eastern Amazonian Landscape, Ecological Applications, 14, 139–149, https://doi.org/10.1890/01-6029, 2004.

Andela, N. and Jones, M. W.: Update of: The Global Fire Atlas of individual fire size, duration, speed and direction, https://doi.org/10.5281/zenodo.11400062, 2024.

Andela, N., Morton, D. C., Schroeder, W., Chen, Y., Brando, P. M., and Randerson, J. T.: Tracking and classifying Amazon fire events in near real time, Science Advances, 8, eabd2713, https://doi.org/10.1126/sciadv.abd2713, 2022.

Andreae, M. O.: Emission of trace gases and aerosols from biomass burning – an updated assessment, Atmospheric Chemistry and Physics, 19, 8523–8546, https://doi.org/10.5194/acp-19-8523-2019, 2019.

Andreae, M. O. and Merlet, P.: Emission of trace gases and aerosols from biomass burning, Global Biogeochemical Cycles, 15, 955–966, https://doi.org/https://doi.org/10.1029/2000GB001382, 2001.

Apituley, A., Pedergnana, M., Sneep, M. J., Veefkin, P., Loyola, D., Landgraf, J., Borsdorff, T., and Mandal, S.: Sentinel-5 precursor/TROPOMI Level 2 Product User Manual Carbon Monoxide, Tech. Rep. SRON-S5P-LEV2-MA-002, https://sentiwiki.copernicus.eu/web/s5p-products#S5P-Products-L2, 2024.

Aragão, L. E. O. C., Anderson, L. O., Fonseca, M. G., Rosan, T. M., Vedovato, L. B., Wagner, F. H., Silva, C. V. J., Silva Junior, C. H. L., Arai, E., Aguiar, A. P., Barlow, J., Berenguer, E., Deeter, M. N., Domingues, L. G., Gatti, L., Gloor, M., Malhi, Y., Marengo, J. A., Miller, J. B., Phillips, O. L., and Saatchi, S.: 21st Century drought-related fires counteract the decline of Amazon deforestation carbon emissions, Nature Communications, 9, 536, https://doi.org/10.1038/s41467-017-02771-y, 2018.

Arellano, A. F., Kasibhatla, P. S., Giglio, L., van der Werf, G. R., Randerson, J. T., and Collatz, G. J.: Time-dependent inversion estimates of global biomass-burning CO emissions using Measurement of Pollution in the Troposphere (MOPITT) measurements, Journal of Geophysical Research: Atmospheres, 111, https://doi.org/10.1029/2005JD006613, 2006.

Arruda, D., Candido, H. G., and Fonseca, R.: Amazon fires threaten Brazil's agribusiness, Science, 365, 1387–1387, https://doi.org/10.1126/science.aaz2198, 2019.

Barlow, J., Lennox, G. D., Ferreira, J., Berenguer, E., Lees, A. C., Nally, R. M., Thomson, J. R., Ferraz, S. F. d. B., Louzada, J., Oliveira, V. H. F., Parry, L., Ribeiro de Castro Solar, R., Vieira, I. C. G., Aragão, L. E. O. C., Begotti, R. A., Braga, R. F., Cardoso, T. M., de Oliveira, R. C., Souza Jr, C. M., Moura, N. G., Nunes, S. S., Siqueira, J. V., Pardini, R., Silveira, J. M., Vaz-de Mello, F. Z., Veiga, R. C. S., Venturieri, A., and Gardner, T. A.: Anthropogenic disturbance in tropical forests can double biodiversity loss from deforestation, Nature, 535, 144–147, https://doi.org/10.1038/nature18326, 2016.

Barlow, J., Berenguer, E., Carmenta, R., and França, F.: Clarifying Amazonia's burning crisis, Global Change Biology, 26, 319–321, https://doi.org/https://doi.org/10.1111/gcb.14872, 2020.

https://doi.org/10.5194/egusphere-2025-6213
Preprint. Discussion started: 5 February 2026

Basso, L. S., Wilson, C., Chipperfield, M. P., Tejada, G., Cassol, H. L. G., Arai, E., Williams, M., Smallman, T. L., Peters, W., Naus, S., Miller, J. B., and Gloor, M.: Atmospheric CO_2 inversion reveals the Amazon as a minor carbon source caused by fire emissions, with forest uptake offsetting about half of these emissions, Atmospheric Chemistry and Physics, 23, 9685–9723, https://doi.org/10.5194/acp-23-9685-2023, 2023.

Basu, S., Baker, D. F., Chevallier, F., Patra, P. K., Liu, J., and Miller, J. B.: The impact of transport model differences on CO_2 surface flux estimates from OCO-2 retrievals of column average CO_2, Atmospheric Chemistry and Physics, 18, 7189–7215, https://doi.org/10.5194/acp-18-7189-2018, 2018.

Bergamaschi, P., Hein, R., Heimann, M., and Crutzen, P. J.: Inverse modeling of the global CO cycle: 1. Inversion of CO mixing ratios, Journal of Geophysical Research: Atmospheres, 105, 1909–1927, https://doi.org/10.1029/1999JD900818, 2000.

Bergamaschi, P., Frankenberg, C., Meirink, J. F., Krol, M., Villani, M. G., Houweling, S., Dentener, F., Dlugokencky, E. J., Miller, J. B., Gatti, L. V., Engel, A., and Levin, I.: Inverse modeling of global and regional CH4 emissions using SCIAMACHY satellite retrievals, Journal of Geophysical Research: Atmospheres, 114, https://doi.org/10.1029/2009JD012287, 2009.

Bloom, A. A., Worden, J., Jiang, Z., Worden, H., Kurosu, T., Frankenberg, C., and Schimel, D.: Remote-sensing constraints on South America fire traits by Bayesian fusion of atmospheric and surface data, Geophysical Research Letters, 42, 1268–1274, https://doi.org/10.1002/2014GL062584, 2015.

Borsdorff, T., aan de Brugh, J., Hu, H., Hasekamp, O., Sussmann, R., Rettinger, M., Hase, F., Gross, J., Schneider, M., Garcia, O., Stremme, W., Grutter, M., Feist, D. G., Arnold, S. G., De Mazière, M., Kumar Sha, M., Pollard, D. F., Kiel, M., Roehl, C., Wennberg, P. O., Toon, G. C., and Landgraf, J.: Mapping carbon monoxide pollution from space down to city scales with daily global coverage, Atmospheric Measurement Techniques, 11, 5507–5518, https://doi.org/10.5194/amt-11-5507-2018, 2018.

Botía, S., Munassar, S., Koch, T., Custodio, D., Basso, L. S., Komiya, S., Lavric, J. V., Walter, D., Gloor, M., Martins, G., Naus, S., Koren, G., Luijkx, I. T., Hantson, S., Miller, J. B., Peters, W., Rödenbeck, C., and Gerbig, C.: Combined CO_2 measurement record indicates Amazon forest carbon uptake is offset by savanna carbon release, Atmospheric Chemistry and Physics, 25, 6219–6255, https://doi.org/10.5194/acp-25-6219-2025, 2025.

Bourgoin, C., Ceccherini, G., Girardello, M., Vancutsem, C., Avitabile, V., Beck, P. S. A., Beuchle, R., Blanc, L., Duveiller, G., Migliavacca, M., Vieilledent, G., Cescatti, A., and Achard, F.: Human degradation of tropical moist forests is greater than previously estimated, Nature, 631, 570–576, https://doi.org/10.1038/s41586-024-07629-0, 2024.

Bowman, K. W., Liu, J., Bloom, A. A., Parazoo, N. C., Lee, M., Jiang, Z., Menemenlis, D., Gierach, M. M., Collatz, G. J., Gurney, K. R., and Wunch, D.: Global and Brazilian Carbon Response to El Niño Modoki 2011–2010, Earth and Space Science, 4, 637–660, https://doi.org/10.1002/2016EA000204, 2017.

Brando, P., Macedo, M., Silvério, D., Rattis, L., Paolucci, L., Alencar, A., Coe, M., and Amorim, C.: Amazon wildfires: Scenes from a foreseeable disaster, Flora, 268, 151 609, https://doi.org/https://doi.org/10.1016/j.flora.2020.151609, 2020a.

Brando, P. M., Balch, J. K., Nepstad, D. C., Morton, D. C., Putz, F. E., Coe, M. T., Silvério, D., Macedo, M. N., Davidson, E. A., Nóbrega, C. C., Alencar, A., and Soares-Filho, B. S.: Abrupt increases in Amazonian tree mortality due to drought–fire interactions, Proceedings of the National Academy of Sciences, 111, 6347–6352, https://doi.org/10.1073/pnas.1305499111, 2014.

Brando, P. M., Soares-Filho, B., Rodrigues, L., Assunção, A., Morton, D., Tuchschneider, D., Fernandes, E. C. M., Macedo, M. N., Oliveira, U., and Coe, M. T.: The gathering firestorm in southern Amazonia, Science Advances, 6, eaay1632, https://doi.org/10.1126/sciadv.aay1632, 2020b.

Brienen, R. J. W., Phillips, O. L., Feldpausch, T. R., Gloor, E., Baker, T. R., Lloyd, J., Lopez-Gonzalez, G., Monteagudo-Mendoza, A., Malhi, Y., Lewis, S. L., Vásquez Martinez, R., Alexiades, M., Álvarez Dávila, E., Alvarez-Loayza, P., Andrade, A., Aragão, L. E. O. C., Araujo-Murakami, A., Arets, E. J. M. M., Arroyo, L., Aymard C., G. A., Bánki, O. S., Baraloto, C., Barroso, J., Bonal, D., Boot, R. G. A., Camargo, J. L. C., Castilho, C. V., Chama, V., Chao, K. J., Chave, J., Comiskey, J. A., Cornejo Valverde, F., da Costa, L., de Oliveira, E. A., Di Fiore, A., Erwin, T. L., Fauset, S., Forsthofer, M., Galbraith, D. R., Grahame, E. S., Groot, N., Hérault, B., Higuchi, N., Honorio Coronado, E. N., Keeling, H., Killeen, T. J., Laurance, W. F., Laurance, S., Licona, J., Magnussen, W. E., Marimon, B. S., Marimon-Junior, B. H., Mendoza, C., Neill, D. A., Nogueira, E. M., Núñez, P., Pallqui Camacho, N. C., Parada, A., Pardo-Molina, G., Peacock, J., Peña-Claros, M., Pickavance, G. C., Pitman, N. C. A., Poorter, L., Prieto, A., Quesada, C. A., Ramírez, F., Ramírez-Angulo, H., Restrepo, Z., Roopsind, A., Rudas, A., Salomão, R. P., Schwarz, M., Silva, N., Silva-Espejo, J. E., Silveira, M., Stropp, J., Talbot, J., ter Steege, H., Teran-Aguilar, J., Terborgh, J., Thomas-Caesar, R., Toledo, M., Torello-Raventos, M., Umetsu, R. K., van der Heijden, G. M. F., van der Hout, P., Guimarães Vieira, I. C., Vieira, S. A., Vilanova, E., Vos, V. A., and Zagt, R. J.: Long-term decline of the Amazon carbon sink, Nature, 519, 344–348, https://doi.org/10.1038/nature14283, 2015.

Brühl, C. and Crutzen, P. J.: MPIC two-dimensional model, NASA Ref. Publ, 1292, 103–104, 1993.

Byrne, B., Liu, J., Lee, M., Yin, Y., Bowman, K. W., Miyazaki, K., Norton, A. J., Joiner, J., Pollard, D. F., Griffith, D. W. T., Velazco, V. A., Deutscher, N. M., Jones, N. B., and Paton-Walsh, C.: The Carbon Cycle of Southeast Australia During 2019–2020: Drought, Fires, and Subsequent Recovery, AGU Advances, 2, e2021AV000 469, https://doi.org/https://doi.org/10.1029/2021AV000469, 2021.

Byrne, B., Liu, J., Bowman, K. W., Pascolini-Campbell, M., Chatterjee, A., Pandey, S., Miyazaki, K., van der Werf, G. R., Wunch, D., Wennberg, P. O., Roehl, C. M., and Sinha, S.: Carbon emissions from the 2023 Canadian wildfires, Nature, 633, 835–839, https://doi.org/10.1038/s41586-024-07878-z, 2024.

Canadian Space Agency: About MOPITT, https://www.asc-csa.gc.ca/eng/satellites/mopitt.asp, last Modified: 2025-05-26, 2025.

Cardil, A., de Miguel, S., Silva, C. A., Reich, P. B., Calkin, D., Brancalion, P. H. S., Vibrans, A. C., Gamarra, J. G. P., Zhou, M., Pijanowski, B. C., Hui, C., Crowther, T. W., Hérault, B., Piotto, D., Salas-Eljatib, C., Broadbent, E. N., Almeyda Zambrano, A. M., Picard, N., Aragão, L. E. O. C., Bastin, J.-F., Routh, D., van den Hoogen, J., Peri, P. L., and Liang, J.: Recent deforestation drove the spike in Amazonian fires, Environmental Research Letters, 15, 121 003, https://doi.org/10.1088/1748-9326/abcac7, 2020.

Chen, Y., Hall, J., Van Wees, D., Andela, N., Hantson, S., Giglio, L., Van Der Werf, G. R., Morton, D. C., and Randerson, J. T.: Multi-decadal trends and variability in burned area from the fifth version of the Global Fire Emissions Database (GFED5), Earth System Science Data, 15, 5227–5259, https://doi.org/10.5194/essd-15-5227-2023, 2023.

Chevallier, F., Fortems, A., Bousquet, P., Pison, I., Szopa, S., Devaux, M., and Hauglustaine, D. A.: African CO emissions between years 2000 and 2006 as estimated from MOPITT observations, Biogeosciences, 6, 103–111, https://doi.org/10.5194/bg-6-103-2009, 2009.

Cochrane, M. A.: Fire science for rainforests, Nature, 421, 913–919, https://doi.org/10.1038/nature01437, 2003.

Copernicus Atmosphere Monitoring Service: CAMS global reanalysis (EAC4). Copernicus Atmosphere Monitoring Service (CAMS) Atmosphere Data Store, https://doi.org/10.24381/d58bbf47, 2020.

Deeter, M., Francis, G., Gille, J., Mao, D., Martínez-Alonso, S., Worden, H., Ziskin, D., Drummond, J., Commane, R., Diskin, G., and McKain, K.: The MOPITT Version 9 CO product: sampling enhancements and validation, Atmospheric Measurement Techniques, 15, 2325–2344, https://doi.org/10.5194/amt-15-2325-2022, 2022.

Deeter, M. N., Emmons, L. K., Francis, G. L., Edwards, D. P., Gille, J. C., Warner, J. X., Khattatov, B., Ziskin, D., Lamarque, J.-F., Ho, S.-P., Yudin, V., Attié, J.-L., Packman, D., Chen, J., Mao, D., and Drummond, J. R.: Operational carbon monoxide retrieval algorithm and selected results for the MOPITT instrument, Journal of Geophysical Research: Atmospheres, 108, https://doi.org/10.1029/2002JD003186, 2003.

Dinerstein, E., Olson, D., Joshi, A., Vynne, C., Burgess, N. D., Wikramanayake, E., Hahn, N., Palminteri, S., Hedao, P., Noss, R., Hansen, M., Locke, H., Ellis, E. C., Jones, B., Barber, C. V., Hayes, R., Kormos, C., Martin, V., Crist, E., Sechrest, W., Price, L., Baillie, J. E. M., Weeden, D., Suckling, K., Davis, C., Sizer, N., Moore, R., Thau, D., Birch, T., Potapov, P., Turubanova, S., Tyukavina, A., de Souza, N., Pintea, L., Brito, J. C., Llewellyn, O. A., Miller, A. G., Patzelt, A., Ghazanfar, S. A., Timberlake, J., Klöser, H., Shennan-Farpón, Y., Kindt, R., Lillesø, J.-P. B., van Breugel, P., Graudal, L., Voge, M., Al-Shammari, K. F., and Saleem, M.: An Ecoregion-Based Approach to Protecting Half the Terrestrial Realm, BioScience, 67, 534–545, https://doi.org/10.1093/biosci/bix014, 2017.

Drummond, J. R. and Mand, G. S.: The Measurements of Pollution in the Troposphere (MOPITT) Instrument: Overall Performance and Calibration Requirements, Journal of Atmospheric and Oceanic Technology, 13, 314–320, https://doi.org/10.1175/1520-0426(1996)013<0314:TMOPIT>2.0.CO;2, 1996.

Eames, T., Kaluka, A., Vernooij, R., Yates, C., Russell-Smith, J., and Van Der Werf, G. R.: A bottom–up savanna fire fuel consumption inventory and its application to savanna burning in Kafue National Park, Zambia, International Journal of Wildland Fire, 34, https://doi.org/10.1071/WF24121, 2025.

Escobar, H.: Amazon fires clearly linked to deforestation, scientists say, Science, 365, 853–853, https://doi.org/10.1126/science.365.6456.853, 2019.

Ferreira, V., Buras, A., Zscheischler, J., Mahecha, M., and Rammig, A.: Evaluating the 2023–2024 record dry-hot conditions in the Amazon in the context of historical compound extremes, Environmental Research Letters, 20, 084 055, https://doi.org/10.1088/1748-9326/ade550, 2025.

Fidelis, A., Alvarado, S. T., Barradas, A. C. S., and Pivello, V. R.: The Year 2017: Megafires and Management in the Cerrado, Fire, 1, 49, https://doi.org/10.3390/fire1030049, 2018.

Forkel, M., Wessollek, C., Huijnen, V., Andela, N., De Laat, A., Kinalczyk, D., Marrs, C., Van Wees, D., Bastos, A., Ciais, P., Fawcett, D., Kaiser, J. W., Klauberg, C., Kutchartt, E., Leite, R., Li, W., Silva, C., Sitch, S., Goncalves De Souza, J., Zaehle, S., and Plummer, S.: Burning of woody debris dominates fire emissions in the Amazon and Cerrado, Nature Geoscience, https://doi.org/10.1038/s41561-024-01637-5, 2025.

Friedlingstein, P., O'Sullivan, M., Jones, M. W., Andrew, R. M., Hauck, J., Landschützer, P., Le Quéré, C., Li, H., Luijkx, I. T., Olsen, A., Peters, G. P., Peters, W., Pongratz, J., Schwingshackl, C., Sitch, S., Canadell, J. G., Ciais, P., Jackson, R. B., Alin, S. R., Arneth, A., Arora, V., Bates, N. R., Becker, M., Bellouin, N., Berghoff, C. F., Bittig, H. C., Bopp, L., Cadule, P., Campbell, K., Chamberlain, M. A., Chandra, N., Chevallier, F., Chini, L. P., Colligan, T., Decayeux, J., Djeutchouang, L. M., Dou, X., Duran Rojas, C., Enyo, K., Evans, W., Fay, A. R., Feely, R. A., Ford, D. J., Foster, A., Gasser, T., Gehlen, M., Gkritzalis, T., Grassi, G., Gregor, L., Gruber, N., Gürses, \., Harris, I., Hefner, M., Heinke, J., Hurtt, G. C., Iida, Y., Ilyina, T., Jacobson, A. R., Jain, A. K., Jarníková, T., Jersild, A., Jiang, F., Jin, Z., Kato, E., Keeling, R. F., Klein Goldewijk, K., Knauer, J., Korsbakken, J. I., Lan, X., Lauvset, S. K., Lefèvre, N., Liu, Z., Liu, J., Ma, L., Maksyutov, S., Marland, G., Mayot, N., McGuire, P. C., Metzl, N., Monacci, N. M., Morgan, E. J., Nakaoka, S.-I., Neill, C., Niwa, Y., Nützel, T., Olivier, L., Ono, T., Palmer, P. I., Pierrot, D., Qin, Z., Resplandy, L., Roobaert, A., Rosan, T. M., Rödenbeck, C., Schwinger, J., Smallman, T. L., Smith, S. M., Sospedra-Alfonso, R., Steinhoff, T., Sun, Q., Sutton, A. J., Séférian, R., Takao, S., Tatebe, H., Tian, H., Tilbrook, B., Torres, O., Tourigny, E., Tsujino, H., Tubiello, F., van der Werf, G., Wanninkhof, R., Wang, X., Yang, D., Yang, X., Yu, Z., Yuan, W., Yue, X., Zaehle, S., Zeng, N., and Zeng, J.: Global Carbon Budget 2024, Earth System Science Data, 17, 965–1039, https://doi.org/10.5194/essd-17-965-2025, 2025.

Gatti, L. V., Miller, J. B., D'Amelio, M. T. S., Martinewski, A., Basso, L. S., Gloor, M. E., Wofsy, S., and Tans, P.: Vertical profiles of CO_2 above eastern Amazonia suggest a net carbon flux to the atmosphere and balanced biosphere between 2000 and 2009, Tellus B: Chemical and Physical Meteorology, 62, 581, https://doi.org/10.1111/j.1600-0889.2010.00484.x, 2010.

Gatti, L. V., Basso, L. S., Miller, J. B., Gloor, M., Gatti Domingues, L., Cassol, H. L. G., Tejada, G., Aragão, L. E. O. C., Nobre, C., Peters, W., Marani, L., Arai, E., Sanches, A. H., Corrêa, S. M., Anderson, L., Von Randow, C., Correia, C. S. C., Crispim, S. P., and Neves, R. A. L.: Amazonia as a carbon source linked to deforestation and climate change, Nature, 595, 388–393, https://doi.org/10.1038/s41586-021-03629-6, 2021.

Gatti, L. V., Cunha, C. L., Marani, L., Cassol, H. L. G., Messias, C. G., Arai, E., Denning, A. S., Soler, L. S., Almeida, C., Setzer, A., Domingues, L. G., Basso, L. S., Miller, J. B., Gloor, M., Correia, C. S. C., Tejada, G., Neves, R. A. L., Rajao, R., Nunes, F., Filho, B. S. S., Schmitt, J., Nobre, C., Corrêa, S. M., Sanches, A. H., Aragão, L. E. O. C., Anderson, L., Von Randow, C., Crispim, S. P., Silva, F. M., and Machado, G. B. M.: Increased Amazon carbon emissions mainly from decline in law enforcement, Nature, https://doi.org/10.1038/s41586-023-06390-0, 2023.

Gloor, M., Gatti, L., Brienen, R., Feldpausch, T. R., Phillips, O. L., Miller, J., Ometto, J. P., Rocha, H., Baker, T., de Jong, B., Houghton, R. A., Malhi, Y., Aragão, L. E. O. C., Guyot, J.-L., Zhao, K., Jackson, R., Peylin, P., Sitch, S., Poulter, B., Lomas, M., Zaehle, S., Huntingford, C., Levy, P., and Lloyd, J.: The carbon balance of South America: a review of the status, decadal trends and main determinants, Biogeosciences, 9, 5407–5430, https://doi.org/10.5194/bg-9-5407-2012, 2012.

Gonzi, S., Feng, L., and Palmer, P. I.: Seasonal cycle of emissions of CO inferred from MOPITT profiles of CO: Sensitivity to pyroconvection and profile retrieval assumptions, Geophysical Research Letters, 38, https://doi.org/10.1029/2011GL046789, 2011.

Goudar, M., Anema, J. C. S., Kumar, R., Borsdorff, T., and Landgraf, J.: Plume detection and emission estimate for biomass burning plumes from TROPOMI carbon monoxide observations using APE v1.1, Geoscientific Model Development, 16, 4835–4852, https://doi.org/10.5194/gmd-16-4835-2023, 2023.

Granier, C., Darras, S., Gon, H. D. v. d., Doubalova, J., Elguindi, N., Galle, B., Gauss, M., Guevara, M., Jalkanen, J.-P., Kuenen, J., Liousse, C., Quack, B., Simpson, D., and Sindelarova, K.: The Copernicus Atmosphere Monitoring Service global and regional emissions (April 2019 version), Tech. rep., Copernicus Atmosphere Monitoring Service (CAMS), https://doi.org/10.24380/d0bn-kx16., 2019.

Griffin, D., Chen, J., Anderson, K., Makar, P., McLinden, C. A., Dammers, E., and Fogal, A.: Biomass burning CO emissions: exploring insights through TROPOMI-derived emissions and emission coefficients, Atmospheric Chemistry and Physics, 24, 10 159–10 186, https://doi.org/10.5194/acp-24-10159-2024, 2024.

Heald, C. L., Jacob, D. J., Jones, D. B. A., Palmer, P. I., Logan, J. A., Streets, D. G., Sachse, G. W., Gille, J. C., Hoffman, R. N., and Nehrkorn, T.: Comparative inverse analysis of satellite (MOPITT) and aircraft (TRACE-P) observations to estimate Asian sources of carbon monoxide, Journal of Geophysical Research: Atmospheres, 109, https://doi.org/10.1029/2004JD005185, 2004.

Heil, A., Kaiser, J. W., Van der Werf, G. R., Wooster, M. J., Schultz, M. G., and van der Gon, H. D.: Assessment of the real-time fire emissions (GFASv0) by MACC, Tech. rep., European Centre for Medium-Range Weather Forecasts, 2010.

Hersbach, H., Bell, B., Berrisford, P., Hirahara, S., Horányi, A., Muñoz-Sabater, J., Nicolas, J., Peubey, C., Radu, R., Schepers, D., Simmons, A., Soci, C., Abdalla, S., Abellan, X., Balsamo, G., Bechtold, P., Biavati, G., Bidlot, J., Bonavita, M., De Chiara, G., Dahlgren, P., Dee, D., Diamantakis, M., Dragani, R., Flemming, J., Forbes, R., Fuentes, M., Geer, A., Haimberger, L., Healy, S., Hogan, R. J., Hólm, E., Janisková, M., Keeley, S., Laloyaux, P., Lopez, P., Lupu, C., Radnoti, G., De Rosnay, P., Rozum, I., Vamborg, F., Villaume, S., and Thépaut, J.: The ERA5 global reanalysis, Quarterly Journal of the Royal Meteorological Society, 146, 1999–2049, https://doi.org/10.1002/qj.3803, 2020.

Hooghiemstra, P. B., Krol, M. C., Meirink, J. F., Bergamaschi, P., van der Werf, G. R., Novelli, P. C., Aben, I., and Röckmann, T.: Optimizing global CO emission estimates using a four-dimensional variational data assimilation system and surface network observations, Atmospheric Chemistry and Physics, 11, 4705–4723, https://doi.org/10.5194/acp-11-4705-2011, 2011.

Hooghiemstra, P. B., Krol, M. C., van Leeuwen, T. T., van der Werf, G. R., Novelli, P. C., Deeter, M. N., Aben, I., and Röckmann, T.: Interannual variability of carbon monoxide emission estimates over South America from 2006 to 2010, Journal of Geophysical Research: Atmospheres, 117, https://doi.org/10.1029/2012JD017758, 2012.

Hubau, W., Lewis, S. L., Phillips, O. L., Affum-Baffoe, K., Beeckman, H., Cuní-Sanchez, A., Daniels, A. K., Ewango, C. E. N., Fauset, S., Mukinzi, J. M., Sheil, D., Sonké, B., Sullivan, M. J. P., Sunderland, T. C. H., Taedoumg, H., Thomas, S. C., White, L. J. T., Abernethy, K. A., Adu-Bredu, S., Amani, C. A., Baker, T. R., Banin, L. F., Baya, F., Begne, S. K., Bennett, A. C., Benedet, F., Bitariho, R., Bocko, Y. E., Boeckx, P., Boundja, P., Brienen, R. J. W., Brncic, T., Chezeaux, E., Chuyong, G. B., Clark, C. J., Collins, M., Comiskey, J. A., Coomes, D. A., Dargie, G. C., De Haulleville, T., Kamdem, M. N. D., Doucet, J.-L., Esquivel-Muelbert, A., Feldpausch, T. R., Fofanah, A., Foli, E. G., Gilpin, M., Gloor, E., Gonmadje, C., Gourlet-Fleury, S., Hall, J. S., Hamilton, A. C., Harris, D. J., Hart, T. B., Hockemba, M. B. N., Hladik, A., Ifo, S. A., Jeffery, K. J., Jucker, T., Yakusu, E. K., Kearsley, E., Kenfack, D., Koch, A., Leal, M. E., Levesley, A., Lindsell, J. A., Lisingo, J., Lopez-Gonzalez, G., Lovett, J. C., Makana, J.-R., Malhi, Y., Marshall, A. R., Martin, J., Martin, E. H., Mbayu, F. M., Medjibe, V. P., Mihindou, V., Mitchard, E. T. A., Moore, S., Munishi, P. K. T., Bengone, N. N., Ojo, L., Ondo, F. E., Peh, K. S.-H., Pickavance, G. C., Poulsen, A. D., Poulsen, J. R., Qie, L., Reitsma, J., Rovero, F., Swaine, M. D., Talbot, J., Taplin, J., Taylor, D. M., Thomas, D. W., Toirambe, B., Mukendi, J. T., Tuagben, D., Umunay, P. M., Van Der Heijden, G. M. F., Verbeeck, H., Vleminckx, J., Willcock, S., Wöll, H., Woods, J. T., and Zemagho, L.: Asynchronous carbon sink saturation in African and Amazonian tropical forests, Nature, 579, 80–87, https://doi.org/10.1038/s41586-020-2035-0, 2020.

Inness, A., Ades, M., Agusti-Panareda, A., Barré, J., Benedictow, A., Blechschmidt, A.-M., Dominguez, J. J., Engelen, R., Eskes, H., Flemming, J., Huijnen, V., Jones, L., Kipling, Z., Massart, S., Parrington, M., Peuch, V.-H., Razinger, M., Remy, S., Schulz, M., and Suttie, M.: The CAMS reanalysis of atmospheric composition, Atmospheric Chemistry and Physics Discussions, pp. 1–55, https://doi.org/10.5194/acp-2018-1078, 2019.

Jiang, Z., Worden, J. R., Worden, H., Deeter, M., Jones, D. B. A., Arellano, A. F., and Henze, D. K.: A 15-year record of CO emissions constrained by MOPITT CO observations, Atmospheric Chemistry and Physics, 17, 4565–4583, https://doi.org/10.5194/acp-17-4565-2017, 2017.

Jin, Y., Stephens, B. B., Long, M. C., Chandra, N., Chevallier, F., Hooghiem, J. J. D., Luijkx, I. T., Maksyutov, S., Morgan, E. J., Niwa, Y., Patra, P. K., Rödenbeck, C., and Vance, J.: The Atmospheric Potential Oxygen forward Model Intercomparison Project (APO-MIP1): evaluating simulated atmospheric transport of air-sea gas exchange tracers and APO flux products, Geoscientific Model Development, 18, 5937–5969, https://doi.org/10.5194/gmd-18-5937-2025, 2025.

Jolly, W. M., Cochrane, M. A., Freeborn, P. H., Holden, Z. A., Brown, T. J., Williamson, G. J., and Bowman, D. M. J. S.: Climate-induced variations in global wildfire danger from 1979 to 2013, Nature Communications, 6, 7537, https://doi.org/10.1038/ncomms8537, 2015.

Jones, D., Prates, L., Qu, Z., Cheng, W., Miyazaki, K., Sekiya, T., Inness, A., Kumar, R., Tang, X., Worden, H., Koren, G., and Huijen, V.: Assessment of regional and interannual variations in tropospheric ozone in chemical reanalyses, EGUsphere, pp. 1–41, https://doi.org/10.5194/egusphere-2024-3759, 2025.

Jones, D. B. A., Bowman, K. W., Logan, J. A., Heald, C. L., Liu, J., Luo, M., Worden, J., and Drummond, J.: The zonal structure of tropical O_3 and CO as observed by the Tropospheric Emission Spectrometer in November 2004 – Part 1: Inverse modeling of CO emissions, Atmospheric Chemistry and Physics, 9, 3547–3562, https://doi.org/10.5194/acp-9-3547-2009, 2009.

https://doi.org/10.5194/egusphere-2025-6213
Preprint. Discussion started: 5 February 2026

Jones, M. W., Abatzoglou, J. T., Veraverbeke, S., Andela, N., Lasslop, G., Forkel, M., Smith, A. J. P., Burton, C., Betts, R. A., van der Werf, G. R., Sitch, S., Canadell, J. G., Santín, C., Kolden, C., Doerr, S. H., and Le Quéré, C.: Global and Regional Trends and Drivers of Fire Under Climate Change, Reviews of Geophysics, 60, e2020RG000 726, https://doi.org/https://doi.org/10.1029/2020RG000726, 2022.

Kaiser, J. W., Heil, A., Andreae, M. O., Benedetti, A., Chubarova, N., Jones, L., Morcrette, J.-J., Razinger, M., Schultz, M. G., Suttie, M., and van der Werf, G. R.: Biomass burning emissions estimated with a global fire assimilation system based on observed fire radiative power, Biogeosciences, 9, 527–554, https://doi.org/10.5194/bg-9-527-2012, 2012.

Kasibhatla, P., Arellano, A., Logan, J. A., Palmer, P. I., and Novelli, P.: Top-down estimate of a large source of atmospheric carbon monoxide associated with fuel combustion in Asia, Geophysical Research Letters, 29, 6–1–6–4, https://doi.org/10.1029/2002GL015581, 2002.

Kelley, D. I., Burton, C., Huntingford, C., Brown, M. A. J., Whitley, R., and Dong, N.: Technical note: Low meteorological influence found in 2019 Amazonia fires, Biogeosciences, 18, 787–804, https://doi.org/10.5194/bg-18-787-2021, 2021.

Koren, G.: Constraining the exchange of carbon dioxide over the Amazon : new insights from stable isotopes, remote sensing and inverse modeling, Ph.D. thesis, Wageningen University, Wageningen, https://edepot.wur.nl/524771, iSBN: 9789463954389, 2020.

Krol, M., Houweling, S., Bregman, B., van den Broek, M., Segers, A., van Velthoven, P., Peters, W., Dentener, F., and Bergamaschi, P.: The two-way nested global chemistry-transport zoom model TM5: algorithm and applications, Atmospheric Chemistry and Physics, 5, 417–432, https://doi.org/10.5194/acp-5-417-2005, 2005.

Krol, M., Peters, W., Hooghiemstra, P., George, M., Clerbaux, C., Hurtmans, D., McInerney, D., Sedano, F., Bergamaschi, P., El Hajj, M., Kaiser, J. W., Fisher, D., Yershov, V., and Muller, J.-P.: How much CO was emitted by the 2010 fires around Moscow?, Atmospheric Chemistry and Physics, 13, 4737–4747, https://doi.org/10.5194/acp-13-4737-2013, 2013.

Krol, M., De Bruine, M., Killaars, L., Ouwersloot, H., Pozzer, A., Yin, Y., Chevallier, F., Bousquet, P., Patra, P., Belikov, D., Maksyutov, S., Dhomse, S., Feng, W., and Chipperfield, M. P.: Age of air as a diagnostic for transport timescales in global models, Geoscientific Model Development, 11, 3109–3130, https://doi.org/10.5194/gmd-11-3109-2018, 2018.

Lan, X., Thoning, K., Dlugokencky, E., and NOAA Global Monitoring Laboratory: Trends in globally-averaged CH4, N2O, and SF6, https://doi.org/10.15138/P8XG-AA10, 2022.

Landgraf, J., aan de Brugh, J., Scheepmaker, R., Borsdorff, T., Hu, H., Houweling, S., Butz, A., Aben, I., and Hasekamp, O.: Carbon monoxide total column retrievals from TROPOMI shortwave infrared measurements, Atmospheric Measurement Techniques, 9, 4955–4975, https://doi.org/10.5194/amt-9-4955-2016, 2016.

Lapola, D. M., Pinho, P., Barlow, J., Aragão, L. E. O. C., Berenguer, E., Carmenta, R., Liddy, H. M., Seixas, H., Silva, C. V. J., Silva-Junior, C. H. L., Alencar, A. A. C., Anderson, L. O., Armenteras, D., Brovkin, V., Calders, K., Chambers, J., Chini, L., Costa, M. H., Faria, B. L., Fearnside, P. M., Ferreira, J., Gatti, L., Gutierrez-Velez, V. H., Han, Z., Hibbard, K., Koven, C., Lawrence, P., Pongratz, J., Portela, B. T. T., Rounsevell, M., Ruane, A. C., Schaldach, R., da Silva, S. S., von Randow, C., and Walker, W. S.: The drivers and impacts of Amazon forest degradation, Science, 379, eabp8622, https://doi.org/10.1126/science.abp8622, 2023.

Lavric, J. and Walter, D.: Mole fractions of CO, CO2, CH4, https://www.attodata.org/ddm/data/Showdata/118, 2019.

Le Page, Y., Morton, D., Hartin, C., Bond-Lamberty, B., Pereira, J. M. C., Hurtt, G., and Asrar, G.: Synergy between land use and climate change increases future fire risk in Amazon forests, Earth System Dynamics, 8, 1237–1246, https://doi.org/10.5194/esd-8-1237-2017, 2017.

Leite, R. V., Silva, C. A., Broadbent, E. N., Amaral, C. H. d., Liesenberg, V., Almeida, D. R. A. d., Mohan, M., Godinho, S., Cardil, A., Hamamura, C., Faria, B. L. d., Brancalion, P. H. S., Hirsch, A., Marcatti, G. E., Dalla Corte, A. P., Zambrano, A. M. A., Costa, M. B. T. d., Matricardi, E. A. T., Silva, A. L. d., Goya, L. R. R. Y., Valbuena, R., Mendonça, B. A. F. d., Silva Junior, C. H. L., Aragão, L. E.

O. C., García, M., Liang, J., Merrick, T., Hudak, A. T., Xiao, J., Hancock, S., Duncason, L., Ferreira, M. P., Valle, D., Saatchi, S., and Klauberg, C.: Large scale multi-layer fuel load characterization in tropical savanna using GEDI spaceborne lidar data, Remote Sensing of Environment, 268, 112 764, https://doi.org/10.1016/j.rse.2021.112764, 2022.

Lichtig, P., Gaubert, B., Emmons, L. K., Jo, D. S., Callaghan, P., Ibarra-Espinosa, S., Dawidowski, L., Brasseur, G. P., and Pfister, G.: Multiscale CO Budget Estimates Across South America: Quantifying Local Sources and Long Range Transport, Journal of Geophysical Research: Atmospheres, 129, e2023JD040 434, https://doi.org/10.1029/2023JD040434, 2024.

Lizundia-Loiola, J., Pettinari, M. L., and Chuvieco, E.: Temporal Anomalies in Burned Area Trends: Satellite Estimations of the Amazonian 2019 Fire Crisis, Remote Sensing, 12, https://doi.org/10.3390/rs12010151, 2020.

Lovejoy, T. E. and Nobre, C.: Amazon tipping point: Last chance for action, Science Advances, 5, eaba2949, https://doi.org/10.1126/sciadv.aba2949, 2019.

Marengo, J. A., Souza, C. M., Thonicke, K., Burton, C., Halladay, K., Betts, R. A., Alves, L. M., and Soares, W. R.: Changes in Climate and Land Use Over the Amazon Region: Current and Future Variability and Trends, Frontiers in Earth Science, 6, 228, https://doi.org/10.3389/feart.2018.00228, 2018.

Martínez-Alonso, S., Deeter, M. N., Baier, B. C., McKain, K., Worden, H., Borsdorff, T., Sweeney, C., and Aben, I.: Evaluation of MOPITT and TROPOMI carbon monoxide retrievals using AirCore in situ vertical profiles, Atmospheric Measurement Techniques, 15, 4751–4765, https://doi.org/10.5194/amt-15-4751-2022, 2022.

Miller, J. B., Giordane A. Martins, De Souza, R. A. F., and Schuldt, K. N.: Manaus aircraft profile data for the period 2017-2023; obspack_multi-species_1_manaus_profiles_v2.0_2023-09-26, https://doi.org/10.25925/20230922, 2023.

Morton, D. C., DeFries, R. S., Shimabukuro, Y. E., Anderson, L. O., Arai, E., del Bon Espirito-Santo, F., Freitas, R., and Morisette, J.: Cropland expansion changes deforestation dynamics in the southern Brazilian Amazon, Proceedings of the National Academy of Sciences, 103, 14 637–14 641, https://doi.org/10.1073/pnas.0606377103, 2006.

Morton, D. C., Defries, R. S., Randerson, J. T., Giglio, L., Schroeder, W., and Van Der Werf, G. R.: Agricultural intensification increases deforestation fire activity in Amazonia: DEFORESTATION FIRES IN AMAZONIA, Global Change Biology, 14, 2262–2275, https://doi.org/10.1111/j.1365-2486.2008.01652.x, 2008.

Morton, D. C., Le Page, Y., DeFries, R., Collatz, G. J., and Hurtt, G. C.: Understorey fire frequency and the fate of burned forests in southern Amazonia, Philosophical Transactions of the Royal Society B: Biological Sciences, 368, 20120 163, https://doi.org/10.1098/rstb.2012.0163, 2013.

Myriokefalitakis, S., Daskalakis, N., Gkouvousis, A., Hilboll, A., van Noije, T., Williams, J. E., Le Sager, P., Huijnen, V., Houweling, S., Bergman, T., Nüß, J. R., Vrekoussis, M., Kanakidou, M., and Krol, M. C.: Description and evaluation of a detailed gas-phase chemistry scheme in the TM5-MP global chemistry transport model (r112), Geoscientific Model Development, 13, 5507–5548, https://doi.org/10.5194/gmd-13-5507-2020, 2020.

Naus, S., Domingues, L. G., Krol, M., Luijkx, I. T., Gatti, L. V., Miller, J. B., Gloor, E., Basu, S., Correia, C., Koren, G., Worden, H. M., Flemming, J., Pétron, G., and Peters, W.: Sixteen years of MOPITT satellite data strongly constrain Amazon CO fire emissions, Atmospheric Chemistry and Physics, 22, 14 735–14 750, https://doi.org/10.5194/acp-22-14735-2022, 2022.

Nawaz, M. O. and Henze, D. K.: Premature Deaths in Brazil Associated With Long-Term Exposure to PM2.5 From Amazon Fires Between 2016 and 2019, GeoHealth, 4, e2020GH000 268, https://doi.org/10.1029/2020GH000268, 2020.

NCAR: Instrument Status | Atmospheric Chemistry Observations & Modeling, https://www2.acom.ucar.edu/mopitt/status?_ga=2.98866587.489968063.1706626033-1227467495.1698671661, 2024.

Nechita-Banda, N., Krol, M., van der Werf, G. R., Kaiser, J. W., Pandey, S., Huijnen, V., Clerbaux, C., Coheur, P., Deeter, M. N., and Röckmann, T.: Monitoring emissions from the 2015 Indonesian fires using CO satellite data, Philosophical Transactions of the Royal Society B: Biological Sciences, 373, 20170 307, https://doi.org/10.1098/rstb.2017.0307, 2018.

Nguyen, H. M., He, J., and Wooster, M. J.: Biomass burning CO, PM and fuel consumption per unit burned area estimates derived across Africa using geostationary SEVIRI fire radiative power and Sentinel-5P CO data, Atmospheric Chemistry and Physics, 23, 2089–2118, https://doi.org/10.5194/acp-23-2089-2023, 2023.

Nüß, J. R., Daskalakis, N., Piwowarczyk, F. G., Gkouvousis, A., Schneising, O., Buchwitz, M., Kanakidou, M., Krol, M. C., and Vrekoussis, M.: Top-down CO emission estimates using TROPOMI CO data in the TM5-4DVAR (r1258) inverse modeling suit, Geoscientific Model Development, 18, 2861–2890, https://doi.org/10.5194/gmd-18-2861-2025, 2025.

Palmer, P. I., Jacob, D. J., Jones, D. B. A., Heald, C. L., Yantosca, R. M., Logan, J. A., Sachse, G. W., and Streets, D. G.: Inverting for emissions of carbon monoxide from Asia using aircraft observations over the western Pacific, Journal of Geophysical Research: Atmospheres, 108, https://doi.org/10.1029/2003JD003397, 2003.

Parsons, L. A.: Implications of CMIP6 Projected Drying Trends for 21st Century Amazonian Drought Risk, Earth's Future, 8, e2020EF001 608, https://doi.org/10.1029/2020EF001608, 2020.

Peiro, H., Crowell, S., and Moore III, B.: Optimizing 4 years of CO_2 biospheric fluxes from OCO-2 and in situ data in TM5: fire emissions from GFED and inferred from MOPITT CO data, Atmospheric Chemistry and Physics, 22, 15 817–15 849, https://doi.org/10.5194/acp-22-15817-2022, 2022.

Peters, W., Miller, J. B., Whitaker, J., Denning, A. S., Hirsch, A., Krol, M. C., Zupanski, D., Bruhwiler, L., and Tans, P. P.: An ensemble data assimilation system to estimate CO2 surface fluxes from atmospheric trace gas observations, Journal of Geophysical Research: Atmospheres, 110, https://doi.org/10.1029/2005JD006157, 2005.

Pfister, G., Hess, P. G., Emmons, L. K., Lamarque, J.-F., Wiedinmyer, C., Edwards, D. P., Pétron, G., Gille, J. C., and Sachse, G. W.: Quantifying CO emissions from the 2004 Alaskan wildfires using MOPITT CO data, Geophysical Research Letters, 32, https://doi.org/10.1029/2005GL022995, 2005.

Phillips, O. L., Brienen, R. J. W., and the RAINFOR collaboration: Carbon uptake by mature Amazon forests has mitigated Amazon nations' carbon emissions, Carbon Balance and Management, 12, 1, https://doi.org/10.1186/s13021-016-0069-2, 2017.

Pison, I., Bousquet, P., Chevallier, F., Szopa, S., and Hauglustaine, D.: Multi-species inversion of CH_4, CO and H_2 emissions from surface measurements, Atmospheric Chemistry and Physics, 9, 5281–5297, https://doi.org/10.5194/acp-9-5281-2009, 2009.

Pivello, V. R.: The Use of Fire in the Cerrado and Amazonian Rainforests of Brazil: Past and Present, Fire Ecology, 7, 24–39, https://doi.org/10.4996/fireecology.0701024, 2011.

Pétron, G., Granier, C., Khattatov, B., Lamarque, J.-F., Yudin, V., Müller, J.-F., and Gille, J.: Inverse modeling of carbon monoxide surface emissions using Climate Monitoring and Diagnostics Laboratory network observations, Journal of Geophysical Research: Atmospheres, 107, ACH 10–1–ACH 10–23, https://doi.org/10.1029/2001JD001305, 2002.

Pétron, G., Granier, C., Khattatov, B., Yudin, V., Lamarque, J.-F., Emmons, L., Gille, J., and Edwards, D. P.: Monthly CO surface sources inventory based on the 2000–2001 MOPITT satellite data, Geophysical Research Letters, 31, https://doi.org/10.1029/2004GL020560, 2004.

Qin, Y., Xiao, X., Wigneron, J.-P., Ciais, P., Brandt, M., Fan, L., Li, X., Crowell, S., Wu, X., Doughty, R., Zhang, Y., Liu, F., Sitch, S., and Moore, B.: Carbon loss from forest degradation exceeds that from deforestation in the Brazilian Amazon, Nature Climate Change, 11, 442–448, https://doi.org/10.1038/s41558-021-01026-5, 2021.

Ramo, R., Roteta, E., Bistinas, I., van Wees, D., Bastarrika, A., Chuvieco, E., and van der Werf, G. R.: African burned area and fire carbon emissions are strongly impacted by small fires undetected by coarse resolution satellite data, Proceedings of the National Academy of Sciences, 118, e2011160 118, https://doi.org/10.1073/pnas.2011160118, 2021.

Randerson, J. T., Chen, Y., Van Der Werf, G. R., Rogers, B. M., and Morton, D. C.: Global burned area and biomass burning emissions from small fires, Journal of Geophysical Research: Biogeosciences, 117, 2012JG002 128, https://doi.org/10.1029/2012JG002128, 2012.

Remaud, M., Ma, J., Krol, M., Abadie, C., Cartwright, M. P., Patra, P., Niwa, Y., Rodenbeck, C., Belviso, S., Kooijmans, L., Lennartz, S., Maignan, F., Chevallier, F., Chipperfield, M. P., Pope, R. J., Harrison, J. J., Vimont, I., Wilson, C., and Peylin, P.: Intercomparison of Atmospheric Carbonyl Sulfide (TransCom-COS; Part One): Evaluating the Impact of Transport and Emissions on Tropospheric Variability Using Ground-Based and Aircraft Data, Journal of Geophysical Research: Atmospheres, 128, e2022JD037 817, https://doi.org/10.1029/2022JD037817, 2023.

Ribeiro, A. F. S., Santos, L., Randerson, J. T., Uribe, M. R., Alencar, A. A. C., Macedo, M. N., Morton, D. C., Zscheischler, J., Silvestrini, R. A., Rattis, L., Seneviratne, S. I., and Brando, P. M.: The time since land-use transition drives changes in fire activity in the Amazon-Cerrado region, Communications Earth & Environment, 5, 1–11, https://doi.org/10.1038/s43247-024-01248-3, 2024.

Rijsdijk, P., Eskes, H., Dingemans, A., Boersma, K. F., Sekiya, T., Miyazaki, K., and Houweling, S.: Quantifying uncertainties in satellite NO_2 superobservations for data assimilation and model evaluation, Geoscientific Model Development, https://gmd.copernicus.org/articles/18/483/2025/, 2025.

Rosan, T. M., Aragão, L. E. O. C., Oliveras, I., Phillips, O. L., Malhi, Y., Gloor, E., and Wagner, F. H.: Extensive 21st-Century Woody Encroachment in South America's Savanna, Geophysical Research Letters, 46, 6594–6603, https://doi.org/10.1029/2019GL082327, 2019.

Roteta, E., Bastarrika, A., Padilla, M., Storm, T., and Chuvieco, E.: Development of a Sentinel-2 burned area algorithm: Generation of a small fire database for sub-Saharan Africa, Remote Sensing of Environment, 222, 1–17, https://doi.org/10.1016/j.rse.2018.12.011, 2019.

Schuldt, K. N., Aalto, T., Arlyn Andrews, Apadula, F., Arnold, S., Baier, B., BÃ¤ni, L., Bergamaschi, P., Biermann, T., Biraud, S. C., Blot, R., Brand, W. A., Francescopiero Calzolari, Chen, G., Huilin Chen, Colomb, A., Commane, R., Condori, L., Conen, F., Conil, S., Couret, C., Cristofanelli, P., Cuevas, E., Daube, B., Davis, K. J., Delmotte, M., Dickerson, R., DiGangi, J. P., Diskin, G., Elsasser, M., Emmenegger, L., Fischer, M. L., Forster, G., Fuente-Lastra, M., Gehrlein, T., Gerbig, C., Hatakka, J., Heimann, M., Heliasz, M., Heltai, D., Hermans, C., Hermansen, O., Hoheisel, A., Holst, J., Di Iorio, T., Jaffe, D. A., Jordan, A., Karion, A., Kazan, V., Keronen, P., Kneuer, T., Kolari, P., Kominkova, K., Kort, E., Kozlova, E., Krummel, P. B., Kubistin, D., Kumps, N., Langenfelds, R. L., Lanza, A., Laurent, O., Laurila, T., Lavric, J., Lee, J., Lehner, I., Lehtinen, K., Leppert, R., Leskinen, A., Leuenberger, M., Levula, J., Lindauer, M., Lindroth, A., Mikaell Ottosson LÃ¶fvenius, Loh, Z. M., Lopez, M., Lunder, C. R., Mammarella, I., Manca, G., Marek, M. V., Marklund, P., Martin, M. Y., De MaziÃ¨re, M., McKain, K., Meinhardt, F., Jean-Marc Metzger, Miles, N. L., Miller, C. E., Miller, J. B., MÃ¶lder, M., Moossen, H., MÃ¼ller-Williams, J., Myhre, C. L., NÃ©dÃ©lec, P., Obersteiner, F., Peltola, O., Petron, G., Piacentino, S., Pichon, J. M., Pickers, P., Plass-DÃ¼lmer, C., Platt, S. M., Ramonet, M., Xinrong Ren, Richardson, S. J., Louis-Jeremy Rigouleau, Rivas, P. P., Rothe, M., Yves-Alain Roulet, Di Sarra, A. G., Scharfe, D., Scheeren, B., Schmidt, M., Schumacher, M., Seifert, T., Sha, M. K., Shepson, P., Sloop, C. D., Smith, P. D., Steger, D., Steinbacher, M., Stephens, B., Sweeney, C., Taipale, R., Timas, H., Trisolino, P., Turnbull, J., Viner, B., Vitkova, G., Watson, A., De Wekker, S., Weyrauch, D., Wofsy, S. C., Worsey, J., Yver-Kwok, C., Zaehle, S., and Zahn, A.: Multi-laboratory compilation of atmospheric carbon monoxide data for the period 1989-2022; obspack_co_1_GLOBALVIEWplus_v4.0_2024-02-13, https://doi.org/10.25925/20231220, 2024.

Sha, M. K., Langerock, B., Blavier, J.-F. L., Blumenstock, T., Borsdorff, T., Buschmann, M., Dehn, A., De Mazière, M., Deutscher, N. M., Feist, D. G., García, O. E., Griffith, D. W. T., Grutter, M., Hannigan, J. W., Hase, F., Heikkinen, P., Hermans, C., Iraci, L. T., Jeseck, P., Jones, N., Kivi, R., Kumps, N., Landgraf, J., Lorente, A., Mahieu, E., Makarova, M. V., Mellqvist, J., Metzger, J.-M., Morino, I., Nagahama, T., Notholt, J., Ohyama, H., Ortega, I., Palm, M., Petri, C., Pollard, D. F., Rettinger, M., Robinson, J., Roche, S., Roehl, C. M., Röhling, A. N., Rousogenous, C., Schneider, M., Shiomi, K., Smale, D., Stremme, W., Strong, K., Sussmann, R., Té, Y., Uchino, O., Velazco, V. A., Vigouroux, C., Vrekoussis, M., Wang, P., Warneke, T., Wizenberg, T., Wunch, D., Yamanouchi, S., Yang, Y., and Zhou, M.: Validation of methane and carbon monoxide from Sentinel-5 Precursor using TCCON and NDACC-IRWG stations, Atmospheric Measurement Techniques, 14, 6249–6304, https://doi.org/10.5194/amt-14-6249-2021, 2021.

Silva, P. S., Nogueira, J., Rodrigues, J. A., Santos, F. L. M., Pereira, J. M. C., DaCamara, C. C., Daldegan, G. A., Pereira, A. A., Peres, L. F., Schmidt, I. B., and Libonati, R.: Putting fire on the map of Brazilian savanna ecoregions, Journal of Environmental Management, 296, 113 098, https://doi.org/10.1016/j.jenvman.2021.113098, 2021.

Silveira, M. V. F., Petri, C. A., Broggio, I. S., Chagas, G. O., Macul, M. S., Leite, C. C. S. S., Ferrari, E. M. M., Amim, C. G. V., Freitas, A. L. R., Motta, A. Z. V., Carvalho, L. M. E., Silva Junior, C. H. L., Anderson, L. O., and Aragão, L. E. O. C.: Drivers of Fire Anomalies in the Brazilian Amazon: Lessons Learned from the 2019 Fire Crisis, Land, 9, 516, https://doi.org/10.3390/land9120516, 2020.

Sofiev, M., Ermakova, T., and Vankevich, R.: Evaluation of the smoke-injection height from wild-land fires using remote-sensing data, Atmospheric Chemistry and Physics, 12, 1995–2006, https://doi.org/10.5194/acp-12-1995-2012, 2012.

Sofiev, M., Vankevich, R., Ermakova, T., and Hakkarainen, J.: Global mapping of maximum emission heights and resulting vertical profiles of wildfire emissions, Atmospheric Chemistry and Physics, 13, 7039–7052, https://doi.org/10.5194/acp-13-7039-2013, 2013.

Soulie, A., Granier, C., Darras, S., Zilbermann, N., Doumbia, T., Guevara, M., Jalkanen, J.-P., Keita, S., Liousse, C., Crippa, M., Guizzardi, D., Hoesly, R., and Smith, S. J.: Global anthropogenic emissions (CAMS-GLOB-ANT) for the Copernicus Atmosphere Monitoring Service simulations of air quality forecasts and reanalyses, Earth System Science Data, 16, 2261–2279, https://doi.org/10.5194/essd-16-2261-2024, 2024.

Stevens, N., Lehmann, C. E. R., Murphy, B. P., and Durigan, G.: Savanna woody encroachment is widespread across three continents, Global Change Biology, 23, 235–244, https://doi.org/10.1111/gcb.13409, 2017.

TerraBrasilis: Download Files – Terrabrasilis, https://terrabrasilis.dpi.inpe.br/en/download-files/, 2025.

Uhl, C. and Buschbacher, R.: A Disturbing Synergism Between Cattle Ranch Burning Practices and Selective Tree Harvesting in the Eastern Amazon, Biotropica, 17, 265–268, https://doi.org/10.2307/2388588, 1985.

Ukkola, A. M., De Kauwe, M. G., Roderick, M. L., Abramowitz, G., and Pitman, A. J.: Robust future changes in meteorological drought in CMIP6 projections despite uncertainty in precipitation, Geophysical Research Letters, 47, e2020GL087 820, https://doi.org/10.1029/2020GL087820, 2020.

van den Berg, A.-W.: Posterior fire emissions and model code for the CO inversion study on the 2019 Amazonia fires, https://doi.org/10.5281/zenodo.17881657, 2025.

van der Laan-Luijkx, I. T., van der Velde, I. R., van der Veen, E., Tsuruta, A., Stanislawska, K., Babenhauserheide, A., Zhang, H. F., Liu, Y., He, W., Chen, H., Masarie, K. A., Krol, M. C., and Peters, W.: The CarbonTracker Data Assimilation Shell (CTDAS) v1.0: implementation and global carbon balance 2001–2015, Geoscientific Model Development, 10, 2785–2800, https://doi.org/10.5194/gmd-10-2785-2017, 2017.

van der Laan-Luijkx, I. T., van der Velde, I. R., Krol, M. C., Gatti, L. V., Domingues, L. G., Correia, C. S. C., Miller, J. B., Gloor, M., Leeuwen, T. T. v., and Kaiser, J. W.: Response of the Amazon carbon balance to the 2010 drought derived with CarbonTracker South America, Global Biogeochemical Cycles, 29, 1092–1108, 2015.

https://doi.org/10.5194/egusphere-2025-6213
Preprint. Discussion started: 5 February 2026

van der Velde, I. R., van der Werf, G. R., Houweling, S., Eskes, H. J., Veefkind, J. P., Borsdorff, T., and Aben, I.: Biomass burning combustion efficiency observed from space using measurements of CO and NO_2 by the TROPOspheric Monitoring Instrument (TROPOMI), Atmospheric Chemistry and Physics, 21, 597–616, https://doi.org/10.5194/acp-21-597-2021, 2021a.

van der Velde, I. R., van der Werf, G. R., Houweling, S., Maasakkers, J. D., Borsdorff, T., Landgraf, J., Tol, P., van Kempen, T. A., van Hees, R., Hoogeveen, R., Veefkind, J. P., and Aben, I.: Vast CO2 release from Australian fires in 2019–2020 constrained by satellite, Nature, 597, 366–369, https://doi.org/10.1038/s41586-021-03712-y, 2021b.

van der Werf, G. R., Randerson, J. T., Collatz, G. J., Giglio, L., Kasibhatla, P. S., Arellano, A. F., Olsen, S. C., and Kasischke, E. S.: Continental-Scale Partitioning of Fire Emissions During the 1997 to 2001 El Niño/La Niña Period, Science, 303, 73–76, https://doi.org/10.1126/science.1090753, 2004.

van der Werf, G. R., Randerson, J. T., Giglio, L., van Leeuwen, T. T., Chen, Y., Rogers, B. M., Mu, M., van Marle, M. J. E., Morton, D. C., Collatz, G. J., Yokelson, R. J., and Kasibhatla, P. S.: Global fire emissions estimates during 1997–2016, Earth System Science Data, 9, 697–720, https://doi.org/10.5194/essd-9-697-2017, 2017.

van der Werf, G. R., Randerson, J. T., van Wees, D., Chen, Y., Giglio, L., Hall, J., Roland, V., Mu, M., Binte Shahid, S., Barsanti, K. C., Yokelson, R., and Morton, D. C.: Landscape fire emissions from the 5th version of the Global Fire Emissions Database (GFED5), Scientific Data, 12, 1870, https://doi.org/10.1038/s41597-025-06127-w, 2025.

van der Woude, A.: Monitoring and Modelling European Carbon Fluxes Using Atmospheric Observations, Ph.D. thesis, University of Groningen / University of Groningen, https://doi.org/10.33612/diss.1019522470, 2024.

van Leeuwen, T. T., Peters, W., Krol, M. C., and van der Werf, G. R.: Dynamic biomass burning emission factors and their impact on atmospheric CO mixing ratios, Journal of Geophysical Research: Atmospheres, 118, 6797–6815, https://doi.org/https://doi.org/10.1002/jgrd.50478, 2013.

Van Wees, D., Van Der Werf, G. R., Randerson, J. T., Rogers, B. M., Chen, Y., Veraverbeke, S., Giglio, L., and Morton, D. C.: Global biomass burning fuel consumption and emissions at 500 m spatial resolution based on the Global Fire Emissions Database (GFED), Geoscientific Model Development, 15, 8411–8437, https://doi.org/10.5194/gmd-15-8411-2022, 2022.

Veefkind, J. P., Aben, I., McMullan, K., Förster, H., de Vries, J., Otter, G., Claas, J., Eskes, H. J., de Haan, J. F., Kleipool, Q., van Weele, M., Hasekamp, O., Hoogeveen, R., Landgraf, J., Snel, R., Tol, P., Ingmann, P., Voors, R., Kruizinga, B., Vink, R., Visser, H., and Levelt, P. F.: TROPOMI on the ESA Sentinel-5 Precursor: A GMES mission for global observations of the atmospheric composition for climate, air quality and ozone layer applications, Remote Sensing of Environment, 120, 70–83, https://doi.org/10.1016/j.rse.2011.09.027, 2012.

Vernooij, R., Eames, T., Russell-Smith, J., Yates, C., Beatty, R., Evans, J., Edwards, A., Ribeiro, N., Wooster, M., Strydom, T., Giongo, M. V., Borges, M. A., Menezes Costa, M., Barradas, A. C. S., Van Wees, D., and Van Der Werf, G. R.: Dynamic savanna burning emission factors based on satellite data using a machine learning approach, Earth System Dynamics, 14, 1039–1064, https://doi.org/10.5194/esd-14-1039-2023, 2023.

Voshtani, S., Jones, D. B. A., Wunch, D., Pendergrass, D. C., Wennberg, P. O., Pollard, D. F., Morino, I., Ohyama, H., Deutscher, N. M., Hase, F., Sussmann, R., Weidmann, D., Kivi, R., García, O., Té, Y., Chen, J., Anderson, K., Stevens, R., Kondragunta, S., Zhu, A., Worthy, D., Racki, S., McKain, K., Makarova, M. V., Jones, N., Mahieu, E., Cadena-Caicedo, A., Cristofanelli, P., Labuschagne, C., Kozlova, E., Seitz, T., Steinbacher, M., Mahdi, R., and Murata, I.: Quantifying CO emissions from boreal wildfires by assimilating TROPOMI and TCCON observations, Atmospheric Chemistry and Physics, 25, 15 527–15 565, https://doi.org/10.5194/acp-25-15527-2025, 2025.

Wainwright, C. M., Allan, R. P., and Black, E.: Consistent Trends in Dry Spell Length in Recent Observations and Future Projections, Geophysical Research Letters, 49, e2021GL097 231, https://doi.org/10.1029/2021GL097231, 2022.

https://doi.org/10.5194/egusphere-2025-6213
Preprint. Discussion started: 5 February 2026

Whitaker, J. S. and Hamill, T. M.: Ensemble Data Assimilation without Perturbed Observations, Monthly Weather Review, https://journals.ametsoc.org/view/journals/mwre/130/7/1520-0493_2002_130_1913_edawpo_2.0.co_2.xml, 2002.

Williams, J. E., Boersma, K. F., Le Sager, P., and Verstraeten, W. W.: The high-resolution version of TM5-MP for optimized satellite retrievals: description and validation, Geoscientific Model Development, 10, 721–750, https://doi.org/10.5194/gmd-10-721-2017, 2017.

Worden, H. M., Deeter, M. N., Edwards, D. P., Gille, J. C., Drummond, J. R., and Nédélec, P.: Observations of near-surface carbon monoxide from space using MOPITT multispectral retrievals, Journal of Geophysical Research: Atmospheres, 115, 2010JD014 242, https://doi.org/10.1029/2010JD014242, 2010.

Yin, Y., Chevallier, F., Ciais, P., Broquet, G., Fortems-Cheiney, A., Pison, I., and Saunois, M.: Decadal trends in global CO emissions as seen by MOPITT, Atmospheric Chemistry and Physics, 15, 13 433–13 451, https://doi.org/10.5194/acp-15-13433-2015, 2015.

Yin, Y., Ciais, P., Chevallier, F., van der Werf, G. R., Fanin, T., Broquet, G., Boesch, H., Cozic, A., Hauglustaine, D., Szopa, S., and Wang, Y.: Variability of fire carbon emissions in equatorial Asia and its nonlinear sensitivity to El Niño, Geophysical Research Letters, 43, 10, 410–472, 479, https://doi.org/https://doi.org/10.1002/2016GL070971, 2016.

Zheng, B., Chevallier, F., Ciais, P., Yin, Y., and Wang, Y.: On the Role of the Flaming to Smoldering Transition in the Seasonal Cycle of African Fire Emissions, Geophysical Research Letters, 45, 11,998–12,007, https://doi.org/10.1029/2018GL079092, 2018.

Zheng, B., Chevallier, F., Yin, Y., Ciais, P., Fortems-Cheiney, A., Deeter, M. N., Parker, R. J., Wang, Y., Worden, H. M., and Zhao, Y.: Global atmospheric carbon monoxide budget 2000–2017 inferred from multi-species atmospheric inversions, Earth System Science Data, 11, 1411–1436, https://doi.org/10.5194/essd-11-1411-2019, 2019.

Zheng, B., Ciais, P., Chevallier, F., Yang, H., Canadell, J. G., Chen, Y., van der Velde, I. R., Aben, I., Chuvieco, E., Davis, S. J., Deeter, M., Hong, C., Kong, Y., Li, H., Li, H., Lin, X., He, K., and Zhang, Q.: Record-high CO_2 emissions from boreal fires in 2021, Science, 379, 912–917, https://doi.org/10.1126/science.ade0805, 2023.